

Design of a Mooring System for FOWT with Sufficient Yaw Stiffness

Auteur : Alufa, Samson Olorunfemi

Promoteur(s) : Rigo, Philippe

Faculté : Faculté des Sciences appliquées

Diplôme : Master : ingénieur civil mécanicien, à finalité spécialisée en "Advanced Ship Design"

Année académique : 2022-2023

URI/URL : <http://hdl.handle.net/2268.2/19335>

Avertissement à l'attention des usagers :

Tous les documents placés en accès ouvert sur le site le site MatheO sont protégés par le droit d'auteur. Conformément aux principes énoncés par la "Budapest Open Access Initiative"(BOAI, 2002), l'utilisateur du site peut lire, télécharger, copier, transmettre, imprimer, chercher ou faire un lien vers le texte intégral de ces documents, les disséquer pour les indexer, s'en servir de données pour un logiciel, ou s'en servir à toute autre fin légale (ou prévue par la réglementation relative au droit d'auteur). Toute utilisation du document à des fins commerciales est strictement interdite.

Par ailleurs, l'utilisateur s'engage à respecter les droits moraux de l'auteur, principalement le droit à l'intégrité de l'oeuvre et le droit de paternité et ce dans toute utilisation que l'utilisateur entreprend. Ainsi, à titre d'exemple, lorsqu'il reproduira un document par extrait ou dans son intégralité, l'utilisateur citera de manière complète les sources telles que mentionnées ci-dessus. Toute utilisation non explicitement autorisée ci-avant (telle que par exemple, la modification du document ou son résumé) nécessite l'autorisation préalable et expresse des auteurs ou de leurs ayants droit.



POLITÉCNICA



Universität
Rostock



Traditio et Innovatio



SOLENT
UNIVERSITY
SOUTHAMPTON



Zachodniopomorski
Uniwersytet
Techniczny
w Szczecinie



With the support of the
Erasmus+ Programme
of the European Union



Design of a mooring system for FOWT with sufficient yaw stiffness

submitted on 27 August, 2023

by

ALUFA Samson Olorunfemi

Leuvenselaan 55

3300 Tienen

alufasamson@hotmail.com

Student ID No.: S213358

Supervisor:

Griet Decorte

Parkwind nv

Co-supervisor:

Tomás Lopez

Universidad Politecnica de Madrid

First Reviewer:

Pr. Hervé Le Sourne

Research Manager (Structures and Materials), ICAM School of Engineering

35 avenue du champ de manoeuvres

44470 Carquefou

France

Second Reviewer:

Msc., Antonio Medina, Manuel

Junior Researcher at the Polytechnic University of Madrid

Avenida de la Memoria, 4

28040 Madrid

Spain



MASTER THESIS

[This page is intentionally left blank]

Contents

List of Figures	v
List of Tables	vii
List of Abbreviations	ix
DECLARATION OF AUTHORSHIP	x
ABSTRACT	xii
1 INTRODUCTION	1
1.1 Background and Motivation	1
1.2 Problem Statement	3
1.3 Aim and Objectives of the Study	4
1.3.1 Aim	4
1.3.2 Objectives	4
1.4 Outline of the Thesis	4
2 THEORETICAL BACKGROUND	5
2.1 Floating Body	5
2.2 Floating Offshore Wind Turbine Structure Types	6
2.3 Water Wave Theory	7
2.3.1 Linear Wave Theory	7
2.3.2 Region of Applicability of Different Wave Theories	8
2.4 Classification of Hydrodynamic Bodies	9
2.4.1 Radiation and Diffraction Analysis	10
2.4.2 Morison Equation	11
2.5 Mooring Systems	12
2.5.1 Types of Mooring	12
2.5.2 Materials for Mooring	14
2.5.3 Mooring Dynamics	16
2.5.4 Initial Cable Configuration	21
2.5.5 Modelling Fibre Ropes	23
3 METHODOLOGY	25
3.1 Software Selection	25
3.1.1 AutoCAD and Rhinoceros	25
3.1.2 GMSH	25
3.1.3 Capytaine	25
3.1.4 NEMOH	26

3.1.5	BEMRosetta	27
3.1.6	MoorDyn	27
3.1.7	OpenFAST	28
3.1.8	WEC-Sim	28
3.2	WEC-Sim Solution Strategy	29
3.2.1	Boundary Element Method Solution	30
3.2.2	Time Series Solution Methodology with WEC-Sim	31
3.2.3	Coupling with MoorDyn	31
3.3	OpenFAST Solution Strategy	35
3.3.1	HydroDyn Calculation Procedure	36
4	MODEL SETUP AND VERIFICATION	37
4.1	Spar Geometry	37
4.2	Hydrostatics	38
4.3	Meshing	40
4.4	Natural Period	44
4.5	BEM Results	46
4.5.1	Added Mass	46
4.5.2	Radiation Damping	48
4.6	Simulink Model	49
4.7	MoorDyn Data Preparation	50
4.7.1	Mooring Line Global Coordinate	51
4.7.2	Volume-Equivalent Diameter	52
4.7.3	Axial Stiffness	53
4.7.4	Line Internal Damping	54
4.7.5	Transverse Drag Coefficients	54
4.7.6	Tangential Drag Coefficients	54
4.7.7	Transverse and Tangential Added Mass Coefficient	55
4.7.8	Buoy Properties	55
4.7.9	Solver Option and Concluding Remarks	56
4.8	ElastoDyn Input Data	57
4.9	HydroDyn Input Data	59
4.9.1	Time Series	60
4.10	AeroDyn and ServoDyn Input Files	62
4.11	Sample Time Series Solution Run with WEC-Sim	62
5	RESULTS AND DISCUSSION	64
5.1	The Crowfoot Model	64
5.2	The Three Catenary Line Model	66
5.3	Proposal by O. Olsen	69

5.4	Proposed Solution	71
5.4.1	Line Properties and Geometry	71
5.4.2	Yaw Response for Proposed Solution	72
6	CONCLUSION AND RECOMMENDATIONS	75
6.1	Conclusion	75
6.2	Recommendations	75
	ACKNOWLEDGEMENTS	76
	References	77
A	SPAR Concrete Substructure General View	82
B	HYDROSTATICS COMPUTATION	84
C	WEC-Sim radiation solution plots	85
D	Properties of R3 studless chain	87
E	Properties of Polyester line	89
F	MATLAB Code for PSD Plots	91
G	Moodyn Input Files	93
G.1	Crowfoot model	93
G.2	Proposed solution	94
H	Response of platform	95
H.1	Platform Yaw Response to Crowfoot Configuration	95
H.2	Platform Yaw Response to Cantenary Configuration	96

List of Figures

1.1	Cost breakdown of an exemplar wind farm versus distance to shore (Martinez and Iglesias, 2022).	2
1.2	Utsira Nord (Equinor, 2021).	3
2.1	Degrees of freedom of a floating body (Tran and Kim, 2015).	5
2.2	Different floating wind turbine concepts (Ørsted, nd).	6
2.3	Definition of wave (Holthuijsen, 2010).	8
2.4	Approximate regions of applicability of different wave theories Le Méhauté, cited in Benitz et al. (2015).	9
2.5	Different wave force regimes. Redrawn from Chakrabarti (1987).	10
2.6	Solution strategy for a floating problem (Faltinsen, 1993).	11
2.7	Catenary mooring system (Ridge et al., 2010).	12
2.8	Taut mooring (Ridge et al., 2010).	12
2.9	Semi-taut mooring.	13
2.10	Tension leg mooring.	13
2.11	Mooring systems types according the lines distribution (Azcona Armendáriz, 2015).	14
2.12	Mooring line discretization (Hall and Goupee, 2015).	16
2.13	Internal and external forces (Hall and Goupee, 2015).	17
2.14	Mooring line in a local coordinate system (Jonkman, 2007).	21
3.1	Simplified flowchart of the internals of Capytaine solver (Ancellin, 2023).	26
3.2	Global flowchart of NEMOH software (Kurnia and Ducrozet, 2022).	27
3.3	WEC-Sim input parameters (Ruehl, 2017).	29
3.4	Simulink library.	29
3.5	Flow chart of WEC-Sim (Ruehl et al., 2022).	30
3.6	MoorDyn Input file.	32
3.7	Mass spring damper idealisation of the mooring line (Hall, 2015).	33
3.8	FAST control volumes for floating systems (Jonkman and Jonkman, 2016).	35
3.9	HydroDyn Calculation Procedure (Jonkman, 2009).	36
4.1	SPAR Geometry (all dimensions in m).	37
4.2	Non-prismatic part of the SPAR geometry.	38
4.3	Mass displacement vs number of elements.	40
4.4	Percentage difference of the displaced mass.	41
4.5	Heave stiffness against maximum size of element.	42
4.6	Roll stiffness against maximum size of element.	42
4.7	Meshed part.	43
4.8	Natural heave period.	44
4.9	Natural pitch period.	45

4.10	Added mass in sway and surge normalised by (ρ)	46
4.11	Added mass in heave and yaw normalised by (ρ)	47
4.12	Added mass in roll and pitch normalised by (ρ)	47
4.13	Radiation damping in sway and surge normalised by $(\rho\omega)$	48
4.14	Radiation damping in heave and yaw normalised by $(\rho\omega)$	49
4.15	Radiation damping in roll and pitch normalised by $(\rho\omega)$	49
4.16	Simulink model.	50
4.17	Plan view of mooring configuration.	51
4.18	Volume equivalent diameter of polyester lines.	52
4.19	Buoy position (Olsen, 2022).	56
4.20	Surface normal of the meshed part.	59
4.21	Radiation damping in yaw dof (using NEMOH).	60
4.22	Wave time series.	60
4.23	Power spectral density of the wave time series.	61
4.24	Yaw response from WEC-Sim.	63
5.1	Crowfoot catenary mooring line configuration Quallen et al. (2013).	64
5.2	Platform's yaw response for an R3 chain with 175 mm nominal diameter.	65
5.3	Catenary configuration analysis drawing.	66
5.4	Platform's yaw response with catenary configuration for an R3 chain with 175 mm nominal diameter.	67
5.5	Comparing yaw response in crowfoot vs. catenary configuration.	68
5.6	Platform's yaw response with with semi taut configuration [proposal 1 by Olsen (2022)].	69
5.7	Comparing yaw response in crowfoot vs. Olsen (2022) proposal configuration vs. catenary.	70
5.8	Proposed configuration.	71
5.9	Detail of fairlead connection.	72
5.10	Platform's yaw response with with semi taut configuration [proposed solution].	73
5.11	Combined plot of yaw response of proposed solution, Olsen (2022), and crowfoot configuration.	74

List of Tables

2.1	Typical natural periods [s] of deep water floaters (DNV, 2010a).	6
2.2	Qualitative assessment of floating wind turbine concepts (Jonkman and Matha, 2011).	7
2.3	Selected properties of mooring line materials (Weller et al., 2013).	15
2.4	Mooring fibre properties (API, 2014).	16
2.5	Summary of recommended stiffness methods West et al. (2020).	24
3.1	MoorDyn parameter description.	33
4.1	Comparison of hydrostatic parameters between spreadsheet computation and study report.	39
4.2	Weight from study report.	39
4.3	Mooring coordinates.	51
4.4	Typical secant stiffness values [EA, kN] (API, 2001).	53
4.5	Two dimensional drag coefficients, Cd for $Re\ 10^4 - 10^7$ (DNV, 2010b).	54
4.6	Transverse and longitudinal drag coefficients (DNV, 2018b).	55
4.7	Buoy properties.	56
4.8	wind turbine structural mass [in tonnes].	57
4.9	Mass and moment arm for platform cog determination.	57
4.10	Platform inertia property.	58
4.11	Wave spectral moment and peak period.	62
5.1	Nodal coordinates of proposed configuration.	72

[This page is intentionally left blank]

List of Abbreviations

Aramid	Aromatic polyamides
BEM	Boundary Element Method
BEMIO	Boundary element input/output
CAD	computer-aided design
cob	centre of buoyancy
cog	centre of gravity
DLC	Design load case
dll	dynamic linked library
DOF	degree of freedom
DOFs	degrees of freedom
FLS	Fatigue limit state
HMPE	High Modulus polyethylene
LCOE	Levelised Cost of Energy
MATLAB	Matrix Laboratory
MBL	Minimum breaking load
MoorDyn	Mooring system dynamics model
MSL	Mean sea level
nfft	Non-Uniform Fast Fourier Transform
NREL	National renewable energy laboratory
OC3	Offshore Code Comparison Collaboration
PA6	Polyamide 6
PET	Polyethylene Terephthalate
PP	Polypropylene
PSD	Power spectral density
PTO	Power take-off
PTO-Sim	Power take-off simulation
QTF	Quadratic transfer function
RAO	Response amplitude operator
TLP	Tension Leg Platform
TLPs	Tension Leg Platforms
WEC-Sim	Wave Energy Converter Simulator
WTG	Wind turbine generator

DECLARATION OF AUTHORSHIP

I, **SAMSON OLORUNFEMI ALUFA** declare that this thesis and the work presented in it are my own and have been generated by me as the result of my own original research.

Where I have consulted the published work of others, this is always clearly attributed.

Where I have quoted from the work of others, the source is always given. With the exception of such quotations, this thesis is entirely my own work.

I have acknowledged all main sources of help.

Where the thesis is based on work done by myself jointly with others, I have made clear exactly what was done by others and what I have contributed myself.

This thesis contains no material that has been submitted previously, in whole or in part, for the award of any other academic degree or diploma.

I cede copyright of the thesis in favour of the Technical University of Madrid (Universidad Politécnica de Madrid) and University of Liege.

Date: August 27, 2023

Signature: 

[This page is intentionally left blank]

ABSTRACT

To further make green energy a mainstay to combat the emissions from the consumption of fossil fuels, alternative solutions for energy generation have been of interest. Offshore wind generation has recently become one of the most promising sustainable energy sources. About 80% of the wind resources are available in offshore regions with water depths of more than 60 m, and using the fixed foundation concept is unfeasible from an economic point of view. The floating wind turbine leverages this abundant wind resource in deep water. One of the critical components of the floating wind turbine is the mooring lines, which keep the floater in place (station keeping). The use of steel chains, polyester, or nylons for the mooring lines is possible. Because of the ease of construction and the unconditional stability offered by the spar-type concept, given that the centre of gravity is lower than the centre of buoyancy, it is used in this study. This report analyses the suitability of taut configuration polyester mooring lines in providing sufficient yaw stiffness for a spar-type floater. The floater is subjected to irregular waves with a water depth of 250 m. The significant wave height and peak periods range from 5.25 m to 6.6 m and 9.03 s to 12.67 s, respectively. In the initial proposed solution, about 95% of the length of each mooring line is made of polyester, while the remaining part is made of stud-less chains with a buoy placed at the connection point; the chain connects to the anchor. A fully coupled analysis is carried out in OpenFAST, and the hydrodynamic input file is prepared with the boundary element method (BEM) solver NEMOH and BEMRosetta. The baseline IEA 15 MW semi-submersible controller and tower properties are used. The MoorDyn program is used to compute the mooring dynamics of the semi-taut mooring configuration. The crowfoot configuration, which is patented, is first modelled, and then the simple catenary system is also modelled. The best configuration is then selected as the one that provides yaw stiffness similar to the crowfoot configuration. The selected configuration is a 3-line semi-taut mooring with three anchor points and six fairlead points. This configuration provides yaw stiffness higher than the initial proposal and utilises 50% less chain and 30% less polyester.

1. INTRODUCTION

1.1. Background and Motivation

Energy, derived from several sources such as nuclear, hydro, petroleum derivatives, solar, and wind, is necessary for human and industrial activities (Abbasi et al., 2021). The ever-increasing energy demand over the years has necessitated the use of petroleum derivatives by the world economy to meet this demand (Wang et al., 2022). Carbon (IV) oxide (CO_2) emission from the consumption of these petroleum derivatives, the main greenhouse gas, reached a record 36.7 million metric tonnes in 2019 (Wang et al., 2022). According to the global energy demand change data, between 2011 and 2018, energy consumption grew by 100% compared to the previous ten years, leading to an increase in fossil fuel energy demand by 2.3% (Abbasi et al., 2021). The emissions and wastes generated by fossil fuel degrade the natural environment (Wang et al., 2022). To solve this issue, the Paris Agreement was set up to maintain global warming to 1.5°C from 2030, which would mean cutting down CO_2 emission by 50% (Abbasi and Adedoyin, 2021).

Reducing carbon emissions has necessitated the rapid development of renewable energies. In recent times, wind energy has gained much attention, and the primary driving force for the rapid growth of offshore wind is the reduction of the Levelized Cost of Energy (LCOE). For an energy project, the LCOE may be defined as the cost of electricity produced over the lifetime of the project (Vazquez and Iglesias, 2016), or the price that the energy must be sold for the project to break even at the end of its design life (Martinez and Iglesias, 2022). The LCOE can also be defined as the cost required to produce one unit of electricity in MW-h over an offshore energy project's design life or life cycle (Musial et al., 2021). The LCOE is a useful first-order metric used to rank different energy sources such as nuclear, combined cycle, and offshore wind (IRENA, 2021). There is an ongoing attempt to further reduce the LCOE by more efficient and economical designs. According to a study by Martinez and Iglesias (2022), the LCOE for floating wind is between 95 €/MWh and about 160 €/MWh. For floating wind turbines in Norway and Portugal, the LCOE for floating offshore wind is around 125 €/MWh.

About 80% of wind resources are located in water depths of more than 60 m (WindEurope, 2017). The limit to water depth of wind turbines with fixed foundations is 50 m for monopiles and more for jackets; however, the jackets are challenging to construct and may not be an optimal solution if high dynamic loads are expected (Shittu et al., 2021). With the limitations of the fixed concept and the prospects of the floating concept in mind, it is imperative to explore the floating offshore wind fully. One of the critical components of the floating offshore wind turbine is the mooring system. Figure 1.1 shows the various costs involved in a floating offshore wind project. The cost presented in Figure 1.1 assumes a fixed water depth of 200 m for the mooring cost. Though the cost of mooring appears

to be the smallest among all the costs in Figure 1.1, this cost increases as the water depth increases (Martinez and Iglesias, 2022) and could reach up to 10% of the total cost of energy (Bhinder et al., 2015). If the construction and manufacturing of load-bearing elements and anchoring technology of a floating offshore wind are improved, then there could be a potential saving in cost of about 14.7% (Kausche et al., 2018). Hence, an efficient foundation design that balances good design and economics is essential.

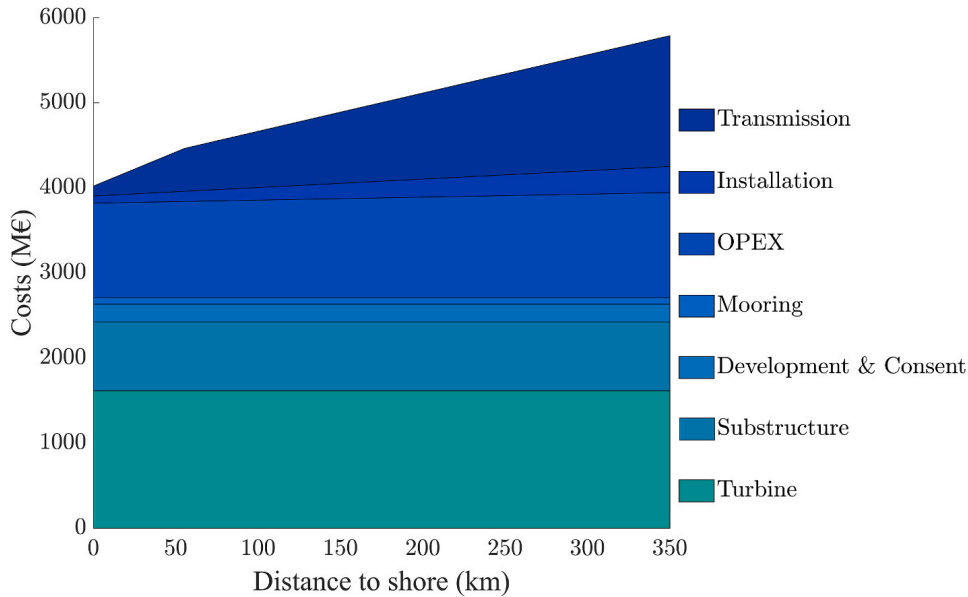


Figure 1.1: Cost breakdown of an exemplar wind farm versus distance to shore (Martinez and Iglesias, 2022).

A spar platform is a deep draft floater usually moored to the seabed, mainly used to support wind turbines. One major issue with the spar floater is the ability of the mooring lines to provide sufficient yaw stiffness. The platform motion is relatively high in yaw (El Beshbichi et al., 2022), and a restraint in this degree of freedom is essential to the smooth operation of the wind turbine. The current optimal solution for mooring configurations is the crowfoot or bridle concept. This concept is patented with CA 2608233 under the Canadian patent; therefore, it can not be used. The bridle concept is a catenary system with three mooring lines that start from the anchor and split into two or more branches close to the fairlead before connecting to the platform. The point of splinting of the line is often referred to as a star-delta connection.

Parkwind nv and NorSea group are accessing the possibility of installing floating offshore wind turbines in Utsira Nord (Figure 1.2) to continue the relentless stride of Norway’s ambition of owning and operating 1 GW of energy by 2030 Equinor (2021) and are seeking an alternative solution to the bridle concept. Utsira Nord is located on the south coast of Norway with a water depth of 250 m at the location where the wind farm will be cited. So, the primary motivation of this work is to design a mooring configuration that is an alternative to the bridle concept and provides a similar level of yaw stiffness. This solution

must be economical, feasible, and timely for the Utsira Nord project.



Figure 1.2: Utsira Nord (Equinor, 2021).

1.2. Problem Statement

The ability of a spar-type floater to provide sufficient yaw stiffness is crucial to the proper functioning of the wind turbine generator (WTG). The WTG cause gyroscopic effects, and the mooring system must be able to restrain the turbine from these gyroscopic effects. The key to achieving this restraint is an efficient mooring design. This work accesses different mooring configurations for the operational design load case (DLC) and selects the best one. The Open-sourced multi-fidelity open-source program OpenFAST, capable of carrying out a complete coupled analysis (aero-servo-hydro-elastic), is used. As part of cost reduction, the major programs used in this study are open source.

1.3. Aim and Objectives of the Study

1.3.1. Aim

The mooring arrangement for the 17 MW floating wind turbine concept has yet to be developed, as no 17 MW wind turbine has been used or deployed commercially. This study aims to design a mooring configuration to provide sufficient yaw stiffness for a spar-type floater to be deployed commercially for the Utsira Nord project.

1.3.2. Objectives

The objectives of this study are to:

- Model the spar geometry in preparation for hydrostatics and hydrodynamics analysis.
- Obtain the hydrostatics properties to verify the values in the study report.
- Carry out a mesh study to determine the meshed part for analysis.
- Analyse the moored platform response to buoy wave elevation records.
- Carry out a fully coupled analysis and compute the yaw response.
- Design the mooring configuration.

1.4. Outline of the Thesis

The remainder of this document has been organised in the following sequence: section 2 describes the relevant background and mathematical formulation of the equations of mooring dynamics and types of mooring lines and configuration used in the floating wind industry; the methodology, and solution strategy is described in section 3; in section 4, the model is prepared for analysis and preliminary results are presented; the main findings and the selected mooring configuration are presented in section 5; and the thesis is finalised with conclusion and recommendation for further work in section 6.

2. THEORETICAL BACKGROUND

2.1. Floating Body

Floating offshore platforms in marine environments are continuously exposed to environmental loads such as waves, currents, and winds, causing the platforms to respond in the 6 degrees of freedom (DOFs), as shown Figure 2.1. The wind turbine can float because of the equilibrium between its mass and the buoyancy force.

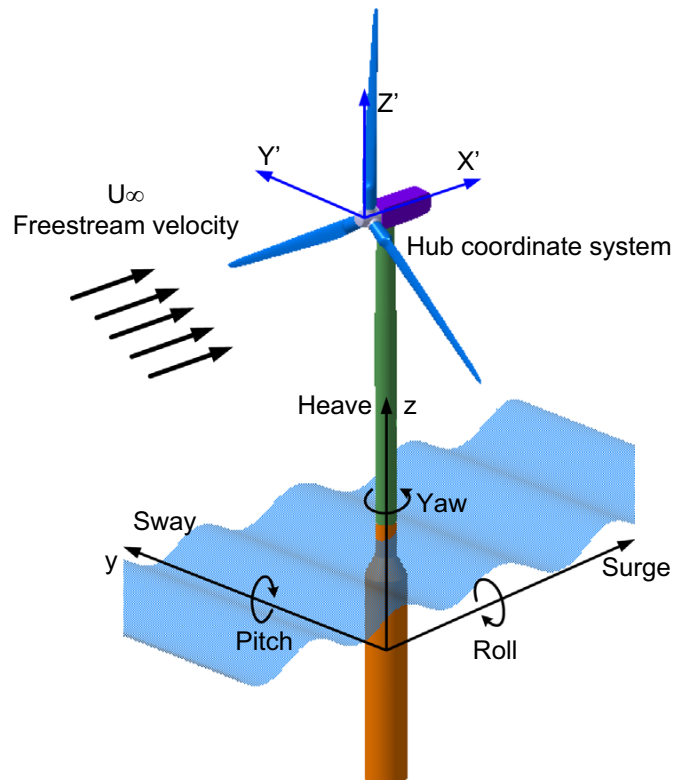


Figure 2.1: Degrees of freedom of a floating body (Tran and Kim, 2015).

According to Faltinsen (1993), the motion of a floating platform may be divided into wave-frequency, high-frequency, mean-drift, and slow-drift. The wave-frequency motion results from the wave-frequency range of significant wave energy, which is linearly excited. The high-frequency motion is caused by a second-order effect, which is significant for tension leg platforms (TLPs) and occurs in the form of *springing* or *ringing* due to resonance oscillation in roll, pitch, and heave of the platform. The high-frequency motion has a natural period of 2-4 s, less than most wave periods and is excited by a non-linear wave effect. Springing and ringing are transient and steady-state oscillations, respectively. The platform's slow-drift and mean drift motions are due to the wave's and wind action's non-linear effect. For a moored platform, the slow drift and mean drift motions occur in the degrees of freedom with neutral stability (surge, sway, yaw), so the restoring force is derived from the mooring lines Faltinsen (1993).

2.2. Floating Offshore Wind Turbine Structure Types

Currently, there are broadly four main types of floating wind turbine floaters. These include the spar, semi-submersible, tension leg platform (TLP), and barge-type floater. The different concepts retain stability in different ways. The spar is ballast stabilised and derives its (rotational) stability from the relative position of the cog and cob. Provided that the cog is lower (closer to the seabed) than the cob, then the spar is stable in pitch and roll. For the semi-submersible and barge-type, the stability in roll and pitch is obtained due to the platform's large water plane area. The larger the water plane, the higher the inertia, translating to greater stability. For the TLPs, the stability of the platform is provided by the rigidity of the tethers. Figure 2.2 shows the different types of concepts.

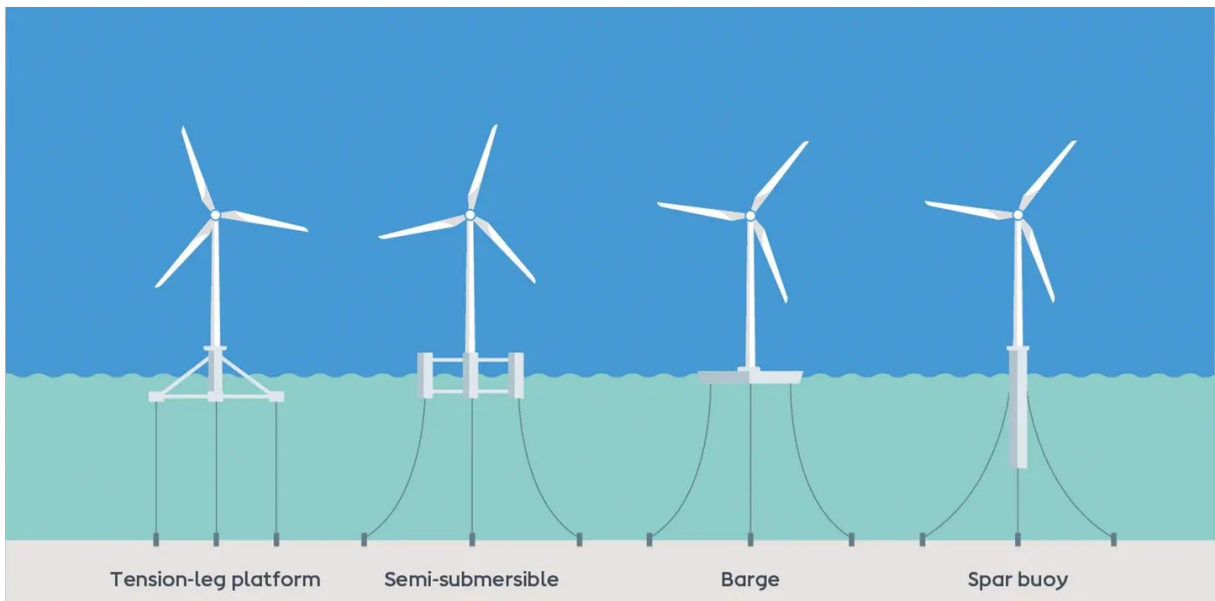


Figure 2.2: Different floating wind turbine concepts (Ørsted, nd).

The typical natural periods of some floating concepts presented in DNV-RP-C205 (DNV, 2010a) are shown in Table 2.1. The low natural periods in heave, roll, and pitch for the TLP explain why the springing and ringing phenomena occur.

Table 2.1: Typical natural periods [s] of deep water floaters (DNV, 2010a).

Floater mode	Spar	TLP	Semi-sub
Surge	> 100	> 100	> 100
Sway	> 100	> 100	> 100
Heave	20 – 35	< 5	20 – 50
Roll	50 – 90	< 5	30 – 60
Pitch	50 – 90	< 5	30 – 60
Yaw	> 100	> 100	> 50 – 60

The various concepts have their peculiarity, and a qualitative assessment according to

Jonkman and Matha (2011) is presented in Table 2.2. In this table, a + indicates that the parameter under consideration is favourable to the floater type, a – sign indicates an unfavourable condition, while 0 means neutral. This is a subjective assessment as noted by Jonkman and Matha (2011); however, one clear thing is that the construction and anchoring are significant issues of the TLPs. The wave sensitivity is relatively better for the spar-buoy since the projected area (perpendicular to the wave direction) is the least of the three concepts of the same power capacity, so the wave incidences are in a relatively small area. Coupled motion is present for the barge type, which is also evident on Table 2.1. Four of the six DOFs have a similar natural period range, meaning two or more of the DOFs may resonate simultaneously.

Table 2.2: Qualitative assessment of floating wind turbine concepts (Jonkman and Matha, 2011).

Parameter	TLP	Spar buoy	Barge
Pitch stability	Mooring	Ballast	Buoyancy
Natural periods	+	0	-
Coupled motion	+	0	-
Wave sensitivity	0	+	-
Turbine weight	0	-	+
Moorings	+	-	-
Anchors	-	+	+
Construction	-	-	+
O&M	+	0	-

2.3. Water Wave Theory

Waves are disturbances that travel through media such as air and water. As waves travel, they carry energy, which is usually dissipated on the structure they come in contact with in whole or in part. In offshore hydrodynamics, the studied waves are usually assumed to be caused by a wind blowing over a fetch whose restoring force is gravity. This wave has a wave period of 1-25 seconds (Benitz et al., 2015). Only the linear wave theory is applied in this study, and this concept is presented next.

2.3.1. Linear Wave Theory

A good understanding of wave modelling is vital before attempting to model or simulate the behaviour of a rigid body in an offshore environment. A more technical definition of waves is required at this point. Before defining a wave, it is essential to understand what *surface elevations* mean and use its meaning to define waves. In a time record, surface elevation is the instantaneous vertical position of the sea surface with respect to some

reference level (Figure 2.3). In such a record, a wave is a profile between two downward or upward zero-crossing elevations (Holthuijsen, 2010).

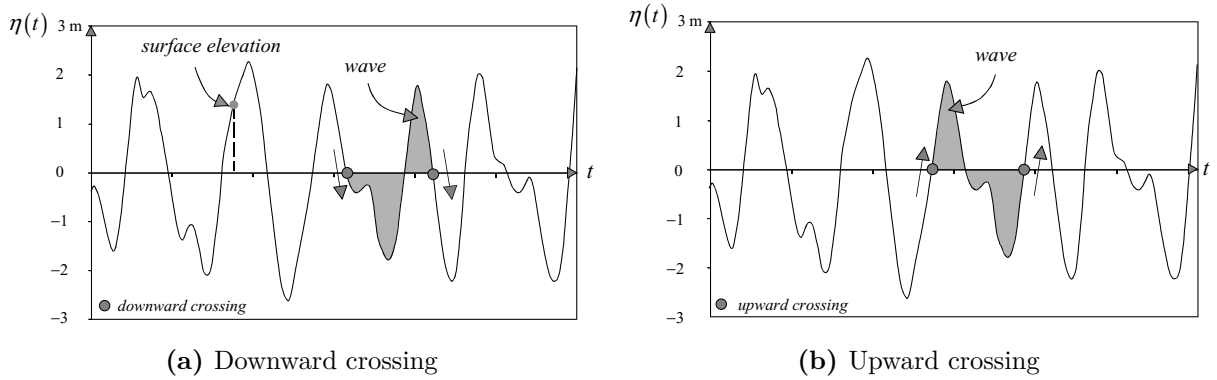


Figure 2.3: Definition of wave (Holthuijsen, 2010).

The linear Airy wave theory is the most practical and straightforward wave theory (Chakrabarti, 1987). This theory is based on the wave height being small compared to the water depth and wavelength. To compute the wave force as a result of this linear wave, it is first assumed that the wave velocity has a potential given by

$$\phi(x, z, t) = \frac{gH}{2kc} \frac{\cosh[k(z+h)]}{\cosh(kh)} \sin[k(x-ct)], \quad (2.1)$$

where g is gravity acceleration, H is wave height, k is wave number, c is wave celerity, h is water depth and ω is the angular frequency of the wave. The pressure from this wave potential is obtained by substituting Equation 2.1 into the unsteady Bernoulli equation (Benitz et al., 2015). After this substitution, it comes:

$$p(x, z, t) = \rho gz + \frac{1}{2} \rho g H \frac{\cosh[k(z+h)]}{\cosh(kh)} \cos(kx - \omega t + \psi) \quad (2.2)$$

The first term of Equation 2.2 represents the static pressure, while the second term represents the dynamic pressure dependent on both time and water depth. Only a very brief introduction to the concept is given here. A more detailed treatment of this subject and all the boundary conditions can be found in Chakrabarti (1987).

2.3.2. Region of Applicability of Different Wave Theories

In hydrodynamic problems, different wave theories are applied. To determine the applicable wave theory for a particular hydrodynamic problem, Le Méhauté's diagram (Figure 2.4) can be used. Figure 2.4 plots the non-dimensionalised wave height against the non-dimensionalised water depth. The combination of the parameters is used to approximate the applicable wave theory. For seas with high wave heights and shallow depths, it is likely that the linear wave theory will not be applicable. However, the linear wave theory could

be applied in a low wave height and deep water. The BEM solvers used in this report apply the linear wave theory in their solution strategy.

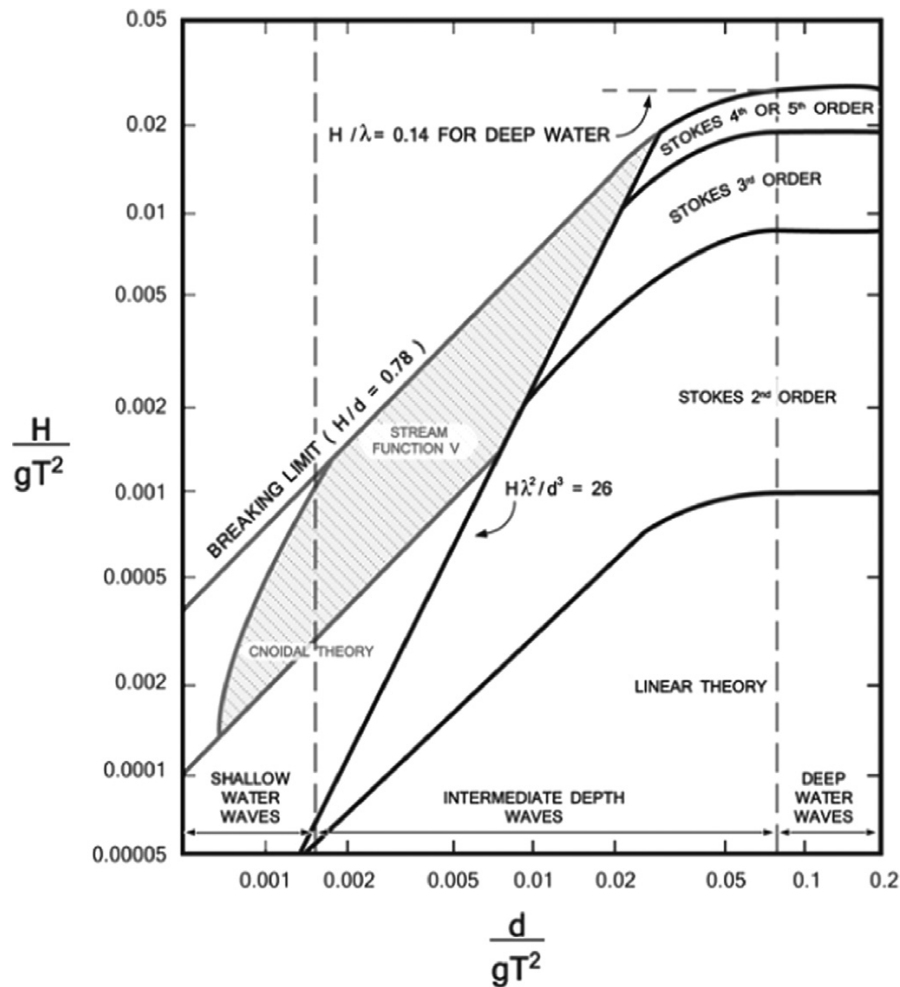


Figure 2.4: Approximate regions of applicability of different wave theories Le Méhauté, cited in Benitz et al. (2015).

2.4. Classification of Hydrodynamic Bodies

In order to compute the wave forces on a hydrodynamic body, it is necessary to know the right approach to adopt. The applicable approach is determined by the ratio of the characteristic dimension of the floating body (D), the sinusoidal wavelength (λ), and the ratio between the wave height (H) and D . Figure 2.5 shows the influence of inertia and drag force on a floating body as determined by the ratios (H/D and $\pi \times D/\lambda$). As seen in Figure 2.5, a floating body with relatively large diameters in deep water will fall under region II, the diffraction region where the structure modifies the flow. For bodies in Region II, the potential flow theory is applicable in determining the wave forces. Slender bodies, such as mooring lines, will most likely fall under region V, which is drag and inertia-dominated, and the structure does not modify the flow. In region V, the Morison

equation is sufficient to determine the wave forces in most cases. In summary, the graph starts from having no influence of drag at all at the bottom right to being drag-dominated at the top right.

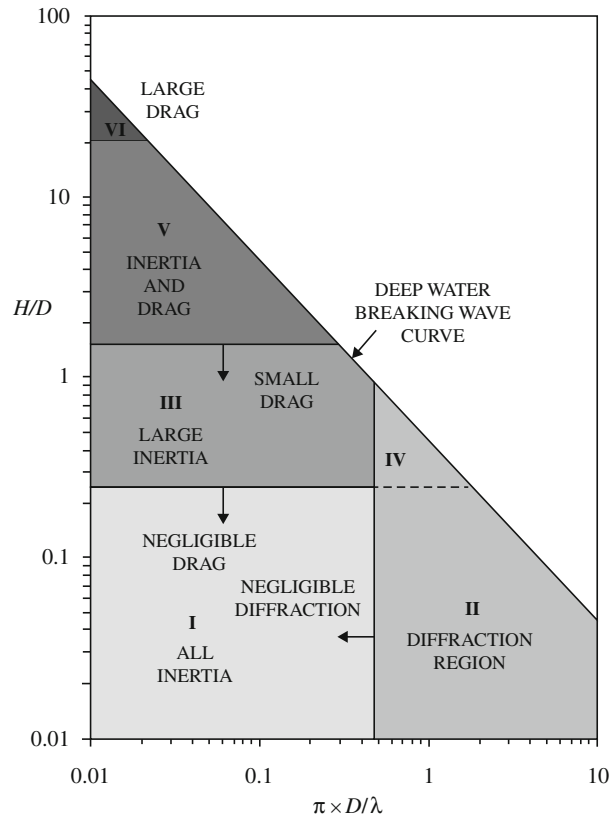


Figure 2.5: Different wave force regimes. Redrawn from Chakrabarti (1987).

2.4.1. Radiation and Diffraction Analysis

The radiation and diffraction theory is used to compute the wave forces of structures in region II of Figure 2.5. The spar considered here falls within the neighbourhood of this region, and it is worth looking at the theory behind this concept. The mathematical formulation can be found in literature such as (Faltinsen, 1993). Only the concept is described here. The radiation and diffraction problem is approached in the following ways: the floating body is assumed to be fixed while the wave progresses towards it (diffraction). As the wave incidents on the platform, two forces emerge. One is the Froude-Krilov force, and the other is the incident wave force. The wave is assumed to be fixed for the radiation while the body oscillates in all DOFs. This results in the added mass and radiation damping in the 6 DOFs. (Figure 2.6) shows how a floating body is idealised and set up for computing the wave forces using the radiation and diffraction approach.

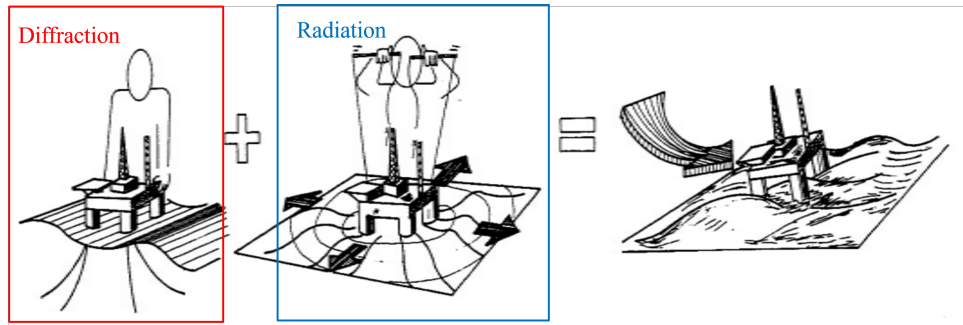


Figure 2.6: Solution strategy for a floating problem (Faltinsen, 1993).

2.4.2. Morison Equation

As noted earlier, the wave forces on the lines are computed using the Morison equation for the mooring lines analysed in this report. A brief introduction to this equation is presented here. When the characteristic diameter of a body is less than $1/4$ to $1/5$ of the wavelength, the effect on the wave is small, and the wave force can be approximated by summing the inertia term and drag term Bergdahl (2017). The drag and inertia forces are linearly added together in the Morison equation, as shown in Equation 2.3. The inertia term consists of the body's mass and the added mass due to water or fluid that is assumed to flow with the body. The drag term is dependent on the relative velocity between the fluid and the body. In the drag term, the relative velocity is of power 2. As shown in Equation 2.3 (the absolute value multiplied by the actual value), it has been written to preserve the correct sign. If it were not written like this, then the product would always be positive, which does not represent what is happening in reality.

$$F = \underbrace{\rho V \frac{du}{dt} - m\ddot{x} + C_m \rho V \left(\frac{du}{dt} - \ddot{x} \right)}_{\text{Inertia term}} + \underbrace{\frac{1}{2} C_D \rho A |u - \dot{x}| (u - \dot{x})}_{\text{Drag term}} \quad (2.3)$$

Where:

- F is the reaction force from the mooring system.
- ρ is the water density.
- The displaced volume is represented by V .
- u and $\frac{du}{dt}$ represent the undisturbed horizontal water velocity and acceleration at the body's centre.
- m represents the mass of the body.
- x , \dot{x} , and \ddot{x} represent the body's position, velocity, and acceleration, respectively, in a direction normal to the relative velocity.
- A is the cross-sectional area of the body.

- C_m and c_D are the added mass- and damping coefficients respectively. Recommended values for C_m and C_D can be found in many references such as DNV-RP-C205 (DNV, 2010a).

2.5. Mooring Systems

2.5.1. Types of Mooring

A mooring system comprises wires, chains and synthetic ropes with one end attached to the vessel or platform and the other fixed to the sea bottom. (Journée and Massie, 2001). According to Journée and Massie (2001), the most common types of mooring systems are:

- Catenary line mooring

In a static sense, this type of mooring configuration gets its restoring force by lifting and lowering the weight of the mooring line, which is predominantly steel.

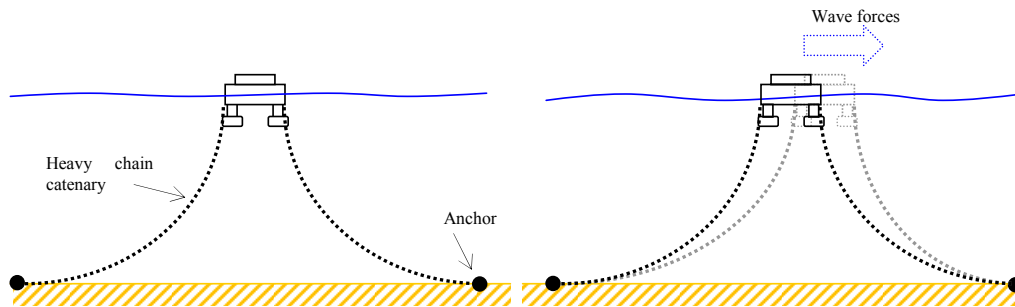


Figure 2.7: Catenary mooring system (Ridge et al., 2010).

- Taut/semi-taut line mooring

The taut line mooring system radiates outward from the floating body to the seabed. The taut mooring is usually made of lightweight materials such as polyester and nylon, so the catenary effect can be considered negligible. The restoring force of the system is obtained as a result of the elastic stiffness of the mooring lines.

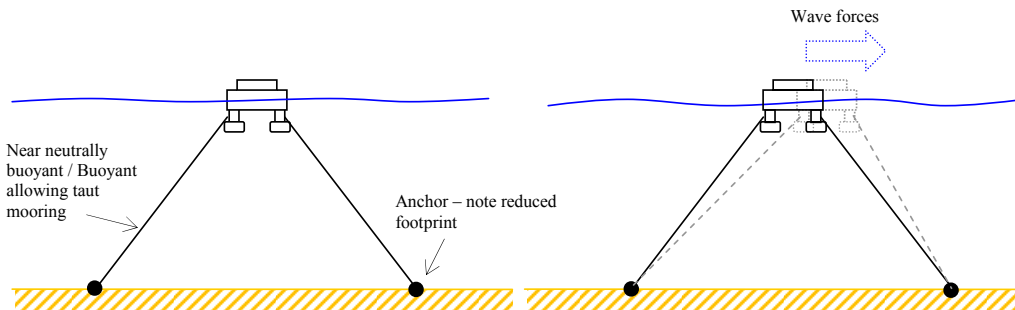


Figure 2.8: Taut mooring (Ridge et al., 2010).

There is also a category of mooring system called the semi-taut mooring. In this type of system, there is usually a combination of chains and ropes. The chains make

contact with the seabed and connect to the anchor. Like the configuration proposed by Olsen (2022), the bottom chain is around 10% of the total line length. The rope connects from the chain to the fairlead. In some configurations, a small chain segment is connected to the fairlead. Sometimes, buoys are placed at the connection point between the chain and the rope as shown in Figure 2.9.

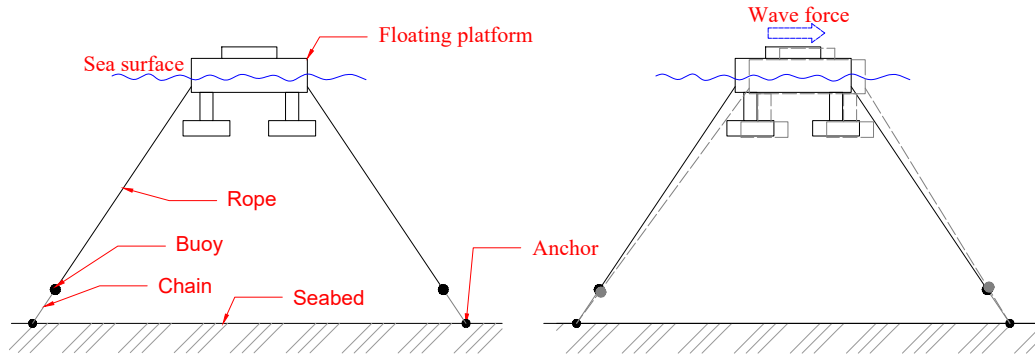


Figure 2.9: Semi-taut mooring.

- Tension leg mooring

This type of mooring system is used for Tension leg platforms (TLP). The buoyancy force on the TLP is greater than the weight of the TLP, so there is a need to counteract the unbalanced force. Since the tension leg mooring always holds down the TLP, the mooring lines will always be under tension. So, when the platform is displaced horizontally, the restoring force results from the horizontal component of the tension in the mooring lines.

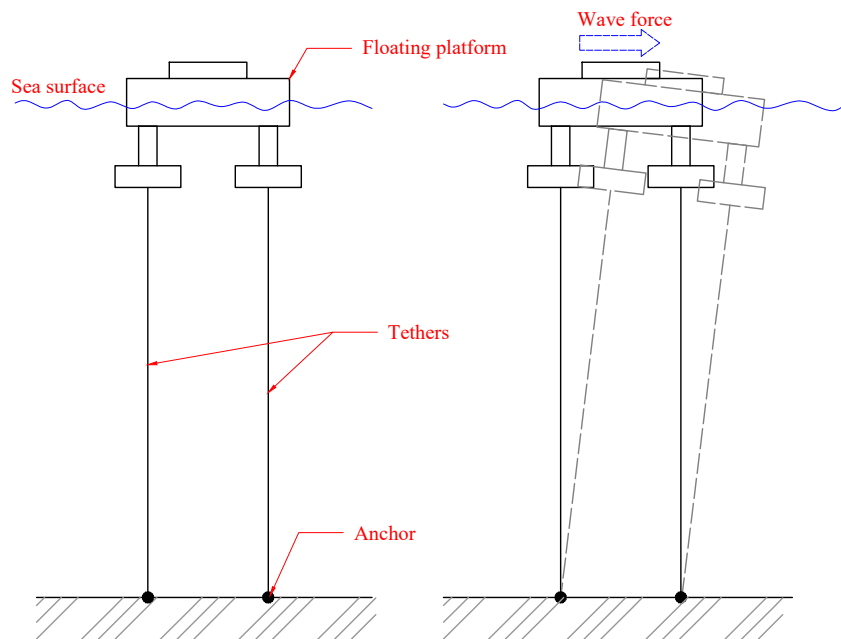


Figure 2.10: Tension leg mooring.

Mooring systems can also be classified based on how they are spread or how the lines are distributed. In Figure 2.11, the equally spread configuration is such that the lines are fixed at unique points on the floater and spread at equal angles; the group spread is such that more than one line is fixed at a point. In contrast, the single spread is such that all the lines connected to the floater all radiate or emanate from one point.

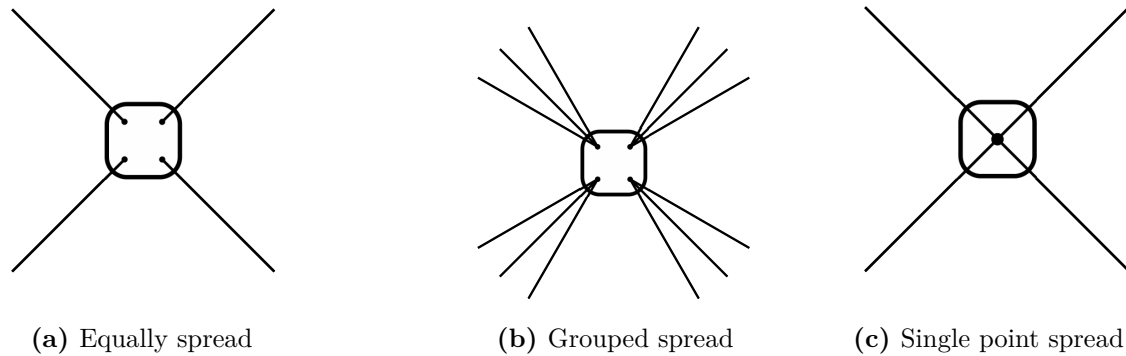


Figure 2.11: Mooring systems types according to the lines distribution (Azcona Armendáriz, 2015).

2.5.2. Materials for Mooring

There are several commercially available materials that could be used for mooring line application. These materials include:

- **Hemp:** According to McKenna et al., (2004) as cited by Weller et al. (2013), natural fibres like hemp has similar strength like nylon and polyester but synthetic materials are favoured as their performance is more predictable in demanding applications including the effects of weathering. Hemp are not commercially used and were used in the early days of sails (Weller et al., 2013).
- **High Modulus polyethylene (HMPE):** The gel spinning of ultra-high molecular weight polyethylene produces HMPE fibers. The concentrated solution-derived extruded gels have the ability to be stretched to produce highly orientated, chain-extended, extremely crystalline fibers. Although the strength and modulus are greater than for Aramids, the low melting point of the fibers (Vlasblom, 2018) and the creep tendencies (ABS, 2021) are drawbacks.
- **Aromatic polyamides (Aramid):** These are high-modulus and high-tenacity fibres. Aramid fibers are relatively light, stiff, and strong . Moreover, they resist impact and abrasion damage, due to the high energy dissipation mechanism involved in their failure (they break into microfibrils). In particular, Aramide fibers are less stiff and strong than carbon, but being lighter, they possess comparable specific strength (strength-to-weight ratio) (Vlasblom, 2018). Their use is quite limited now because of their high cost.

- Polyethylene Terephthalate (PET): This material is the most important polyester. When subjected to quick cooling, PET has the property of being a transparent, amorphous thermoplastic; nevertheless, when cooled slowly or when cold pulled, PET exhibits semicrystalline behavior (Paladhi et al., 2022). They are mostly used in the oil and gas industry.
- Polypropylene (PP): This is a thermoplastic substance utilized in a wide range of products, including textiles, labels, packaging, and home goods. PP is a widely used polymer because of its low cost and great processing ability, especially for the auto sector. At low temperatures, pure PP is resistant to photo-oxidation and thermal oxidation. Additionally, PP is susceptible to a variety of environmental factors, including temperature, light, and radiation (Rani et al., 2023).
- Polyamide 6 (PA6): Nylon 6 and polycaprolactam are additional names for PA6. One of the most widely utilized polyamides on a global scale. It is a versatile and widely used engineering material that offers excellent mechanical properties and resistance to heat, chemicals, and moisture. Its high strength, toughness, and wear resistance make it a popular choice for a wide range of applications in various industries (Team, 2023).

Table 2.3 shows the properties of these materials for comparative purposes.

Table 2.3: Selected properties of mooring line materials (Weller et al., 2013).

Material	Density (g/cm ³)	Moisture (%)	Modulus (N/tex, Gpa)	Strength (Mpa)
Hemp	1.5	8	21.7, 32.6	705
Steel	7.85	0	20, 160	2600
HMPE	0.97	0	100, 100	3400
Aramid	1.45	1-7	60, 90	2900
PET	1.38	<1	11, 15	1130
PP	0.91	0	7, 6	560
PA6	1.14	5	7, 8	960

In the catenary system, chain mooring offers restoring force based on the weight of the chain. This means that heavier chains are required as the water depth increases. There are regions where the weight of the chain becomes impractical because of the length required. Fibre ropes have been used in the oil and gas industry for water depths of up to 3000 m, and their use in the offshore wind industry is gaining popularity. The polyester and nylon lines are two candidates for fibre rope mooring. One major challenge of the fibre rope is internal abrasion from fine particles, which causes strength loss (API, 2014). The particles causing strength loss could come from water with high turbidity (API, 2014) or cable dropping to the sea floor Acteon (2015). Table 2.4 shows comparative properties between the fibre materials used for mooring applications. Based on Table 2.4

and the recommendation of Acteon (2015), the polyester material is preferred over the nylon material since it has better abrasion resistance and tension-tension fatigue damage resistance.

Table 2.4: Mooring fibre properties (API, 2014).

Property	Polyester	Aramid	HMPE	Nylon
Strength to weight ratio	medium	high	high	low
Stiffness	medium	high	high	low
Tension-tension fatigue damage resistance	high	high	high	low ¹
Axial compression fatigue damage resistance	high	low ¹	high	high
Abrasion resistance	high	medium	high	low

¹ The effect of these properties is a function of construction and application.

2.5.3. Mooring Dynamics

Hall and Goupee (2015) presented an approach for computing the dynamics of mooring lines by discretising the mass of the mooring lines as shown in Figure 2.12. In Figure 2.12, the mass of the mooring line is lumped at equal intervals connected by a weightless string. The position of the masses is represented by \mathbf{r}_i with 0 representing the bottom-most node (closer to the anchor) and N at the topmost node (close to the fairlead). \mathbf{r}_i is a vector with components x_i , y_i , and z_i . The connecting string is numbered such that the string connecting nodes i and nodes $i + 1$ are assigned the code number $i + 1/2$. With each segment having the same unstretched length (l), volume-equivalent diameter (d), density (ρ), young modulus (E) and internal damping coefficient (C_{int}). The right-handed inertia frame of reference is used with the z-axis pointing upwards.

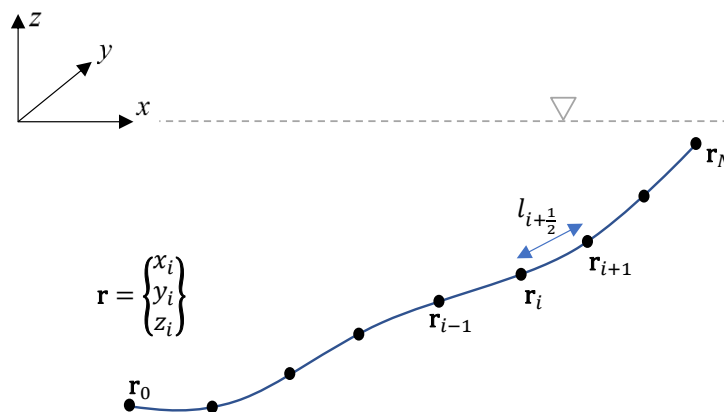


Figure 2.12: Mooring line discretization (Hall and Goupee, 2015).

Though the derivation to be presented here is for a single mooring line with uniform properties, the idea can be extended to mooring lines made of different materials.

The mooring line model combines damping forces with weight and buoyancy forces, internal axial stiffness, hydrodynamic forces from the equation of Morison and forces resulting from contact with seabed (Hall and Goupee, 2015). The various forces are shown in Figure 2.13. The cable weight is lumped at each node i and represented by the downward arrow and \mathbf{W}_i in Figure 2.13. The internal stiffness and mooring line damping are respectively represented as $\mathbf{T}_{i+(1/2)}$ and $\mathbf{C}_{i+(1/2)}$. The tangential direction of the lumped mass at each node may be computed as the average tangent direction of the two adjacent cables as shown in Figure 2.13.

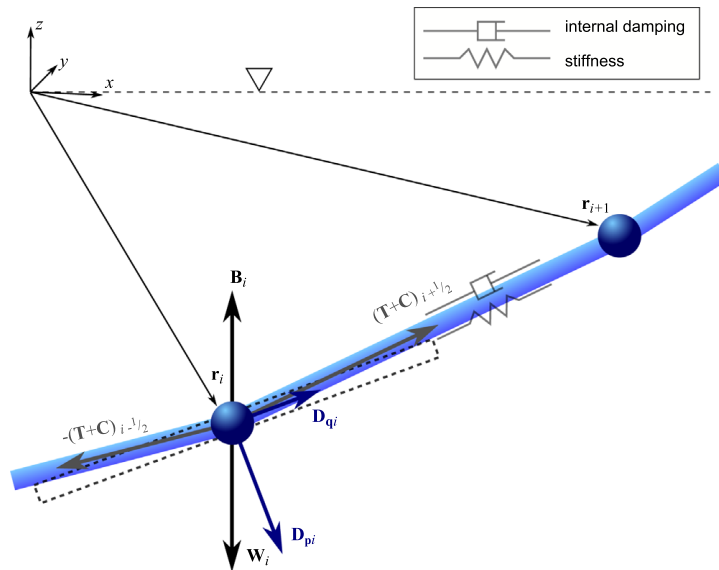


Figure 2.13: Internal and external forces (Hall and Goupee, 2015).

The hydrodynamic forces in the cable are calculated in the mooring line at the node rather than at the midsegment of each line. This is because computing the forces at the node provides damping in all cases. However, when the forces are computed in the mid-segment of the cable, there is an instance when the cable segment does not translate (when cable vibration has a wavelength that is twice the segment length). This will lead to zero damping for this case (Hall and Goupee, 2015). The mooring lines are usually very slender; hence, the shear force may be neglected (Azcona Armendáriz, 2015). The bending and torsional stiffness are also neglected (for mooring lines, the bending stiffness is usually neglected (DNV, 2018b)). In that case, the only internal forces in the cable are tension and damping (Azcona Armendáriz, 2015).

Internal forces

The internal forces included in the mooring discretization are axial stiffness, axial damping, weight, and damping. For convenience, the weight is accounted for together with the internal forces. The resultant vertical force or net buoyancy in each line segment is computed using

$$W_{i+(1/2)} = \frac{\pi}{4} d^2 l (\rho_w - \rho) g, \quad (2.4)$$

Where ρ_w is the density of the fluid (seawater in this case), and g is the gravity acceleration. So the weight at each node may now be computed as the average between the weight of adjacent line segments Hall and Goupee (2015)

$$\mathbf{W}_i = \frac{1}{2} \left(W_{i+(1/2)} + W_{i-(1/2)} \right) \hat{\mathbf{e}}_z \quad (2.5)$$

Where $\hat{\mathbf{e}}_z$ is a unit vector in the positive z direction.

If the bending and torsional stiffness are also neglected, then the only internal force in the cable are tension and damping (Azcona Armendáriz, 2015). The tension in cable segment $i + \frac{1}{2}$ may be represented using the generalised Hooke's law as

$$T_{i+(1/2)} = E \frac{\pi}{4} d^2 \epsilon_{i+(1/2)} \quad (2.6)$$

In Equation 2.6, $\epsilon_{i+(1/2)}$ is the strain which is calculated per segment as the ratio change in length of a segment (stretched length – unstretched length) to the original length of the segment (unstretched length). Since the mooring line is in a 3D space, the stretched length may be represented with an L^2 norm, representing the difference in the node i and node $i + 1$. If this is taken into account and the resulting strain is multiplied by a unit vector pointing in the line segment, then the strain may be obtained as:

$$\epsilon_{i+(1/2)} = \left(\frac{\|\mathbf{r}_{i+1} - \mathbf{r}_i\| - l}{l} \right) \left(\frac{\mathbf{r}_{i+1} - \mathbf{r}_i}{\|\mathbf{r}_{i+1} - \mathbf{r}_i\|} \right) = \left(\frac{1}{l} - \frac{1}{\|\mathbf{r}_{i+1} - \mathbf{r}_i\|} \right) (\mathbf{r}_{i+1} - \mathbf{r}_i) \quad (2.7)$$

Combining Equation 2.6 and Equation 2.7, the tension in the cable may be represented as:

$$\mathbf{T}_{i+(1/2)} = E \frac{\pi}{4} d^2 \left(\frac{1}{l} - \frac{1}{\|\mathbf{r}_{i+1} - \mathbf{r}_i\|} \right) (\mathbf{r}_{i+1} - \mathbf{r}_i) \quad (2.8)$$

In Equation 2.8 a positive L^2 indicates a tensile force, while a negative L^2 indicates a compressive force. For MoorDyn v1 implementation, compressive forces are not considered, so the L^2 norm is penalised so that only values greater than or equal to zero are considered. The next internal force to consider is the internal damping force. Damping forces are usually proportional to velocity, so the internal damping in the cable is proportional to the strain rate. The strain rate is the time derivative of the strain and is a velocity-like entity. Hall and Goupee (2015) presents the internal damping as:

$$\mathbf{C}_{i+(1/2)} = C_{\text{int}} \frac{\pi}{4} d^2 \dot{\epsilon}_{i+(1/2)} \left(\frac{\mathbf{r}_{i+1} - \mathbf{r}_i}{\|\mathbf{r}_{i+1} - \mathbf{r}_i\|} \right) \quad (2.9)$$

The strain rate may be expressed in derivative form as:

$$\dot{\epsilon}_{i+(1/2)} = \frac{\partial \epsilon_{i+(1/2)}}{\partial t} = \frac{\partial}{\partial t} \left(\frac{\|\mathbf{r}_{i+1} - \mathbf{r}_i\|}{l} - 1 \right) \quad (2.10)$$

Equation 2.10 may be simplified thus:

$$\frac{\partial \epsilon_{i+(1/2)}}{\partial t} = \frac{\partial}{\partial t} \left\{ \frac{\|\mathbf{r}_{i+1} - \mathbf{r}_i\|}{l} \right\} - \frac{\partial}{\partial t} \{1\} \quad (2.11)$$

The partial derivative of l w.r.t time Equation 2.11 is zero, so only the first term on the right-hand side will remain. Noting that

$$\|\mathbf{r}_{i+1} - \mathbf{r}_i\| = \sqrt{(x_{i+1} - x_i)^2 + (y_{i+1} - y_i)^2 + (z_{i+1} - z_i)^2}$$

and multiplying Equation 2.11 by

$$\frac{\|\mathbf{r}_{i+1} - \mathbf{r}_i\|}{\|\mathbf{r}_{i+1} - \mathbf{r}_i\|},$$

then dividing the same by 2 to avoid the factor of 2 after taking the derivative obtained:

$$\dot{\epsilon}_{i+(1/2)} = \frac{1}{l} \frac{1}{\|\mathbf{r}_{i+1} - \mathbf{r}_i\|} [(x_{i+1} - x_i)(\dot{x}_{i+1} - \dot{x}_i) + (y_{i+1} - y_i)(\dot{y}_{i+1} - \dot{y}_i) + (z_{i+1} - z_i)(\dot{z}_{i+1} - \dot{z}_i)] \quad (2.12)$$

External forces

The governing equations for the external forces on the mooring lines are derived as presented by (Hall and Goupee, 2015). The hydrodynamic drag and added mass constitute the external forces. So, to consider these forces, the velocity and acceleration of the fluid are resolved to radial and tangential components. It is to be noted that the influence of the wave-particle velocity (wave kinematics) is not taken into account since their effect is negligible on the cables as described by (Hall and Goupee, 2015). The tangential direction of node i may be approximated by considering a line passing through nodes $i - 1$ and $i + 1$. The following unit vector may represent the tangent direction.

$$\hat{\mathbf{q}}_i = \frac{\mathbf{r}_{i+1} - \mathbf{r}_{i-1}}{\|\mathbf{r}_{i+1} - \mathbf{r}_{i-1}\|}, \quad (2.13)$$

So, the transverse direction $\hat{\mathbf{q}}_i$ is perpendicular to direction $\hat{\mathbf{p}}$ and $\hat{\mathbf{p}}$ will always align with the relative direction of the water velocity over the cable. Since still water is being considered (wave kinematics neglected), the relative velocity of the fluid at the node is assumed to be in the opposite direction of the cable. Therefore, the fluid velocity may be represented as the negative derivative of the position vector at the node with respect to time so that the relative water velocity at the node is $-\dot{\mathbf{r}}_i$. The magnitude of the tangential component of this flow is the dot product between $-\dot{\mathbf{r}}_i$ and $\hat{\mathbf{q}}_i$ and is in the

direction of the vector presented in Equation 2.13. Also, the transverse component of the vector is the vector subtraction of the fluid velocity and the tangential component as $(\dot{\mathbf{r}}_i \cdot \hat{\mathbf{q}}_i) \hat{\mathbf{q}}_i - \dot{\mathbf{r}}_i$. Putting these together and considering the drag expression of the Morison equation, the transverse and tangential drag terms may be expressed in the form given in Equation 2.14 and Equation 2.15 respectively.

$$\mathbf{D}_{\mathbf{p}i} = \frac{1}{2} \rho_w C_{dn} dl \|(\dot{\mathbf{r}}_i \cdot \hat{\mathbf{q}}_i) \hat{\mathbf{q}}_i - \dot{\mathbf{r}}_i\| [(\dot{\mathbf{r}}_i \cdot \hat{\mathbf{q}}) \hat{\mathbf{q}}_i - \dot{\mathbf{r}}_i] \quad (2.14)$$

$$\mathbf{D}_{\mathbf{q}i} = \frac{1}{2} \rho_w C_{dt} \pi dl \|(-\dot{\mathbf{r}}_i \cdot \hat{\mathbf{q}}_i) \hat{\mathbf{q}}_i\| (-\dot{\mathbf{r}}_i \cdot \hat{\mathbf{q}}_i) \hat{\mathbf{q}}_i, \quad (2.15)$$

C_{dn} is the transverse drag coefficient while C_{dt} is the tangential drag coefficient. d and l represent the diameter and cable segment length in Equation 2.14 and Equation 2.15 and every other equations within this section.

Similarly, the transverse and tangential added mass, which is a product of the acceleration and the velocity vector, may be computed using Equation 2.16 and Equation 2.17 respectively.

$$\mathbf{a}_{\mathbf{p}i} \mathbf{r}_i = \rho_w C_{an} \frac{\pi}{4} d^2 l [(\ddot{\mathbf{r}}_i \cdot \hat{\mathbf{q}}_i) \hat{\mathbf{q}}_i - \ddot{\mathbf{r}}_i], \quad (2.16)$$

$$\mathbf{a}_{\mathbf{q}i} \ddot{\mathbf{r}}_i = \rho_w C_{at} \frac{\pi}{4} d^2 l (-\ddot{\mathbf{r}}_i \cdot \hat{\mathbf{q}}_i) \hat{\mathbf{q}}_i, \quad (2.17)$$

C_{an} is the transverse added mass coefficient and C_{at} is the tangential added mass coefficient.

To model the forces arising from sea contact, a spring damper model is used, which is only active if the cable makes contact with the seabed ($z_i \leq z_{bot}$). k_b is the spring constant or stiffness coefficient of the seabed, and c_b represents the damping coefficient of the seabed.

$$\mathbf{B}_i = dl [(z_{bot} - z_i) k_b - \dot{z}_i c_b] \hat{\mathbf{e}}_z \quad (2.18)$$

The lumped mass at each node of the mooring line is the sum of one-half the total distributed mass of adjacent line segments. It is possible to represent this mass at each node by a diagonal matrix. To do this, the mass per node is multiplied with a 3×3 identity matrix \mathbf{I} as presented in Equation 2.19

$$m_i = \frac{\pi}{4} d^2 l \rho \mathbf{I}, \quad (2.19)$$

To combine the mass and the added mass, $\ddot{\mathbf{r}}_i$ is factored out from Equation 2.16 and Equation 2.17 and then rearranged to for Equation 2.20.

$$\mathbf{a}_i = \mathbf{a}_{\mathbf{p}i} + \mathbf{a}_{\mathbf{q}i} = \rho_w \frac{\pi}{4} d^2 l \left[C_{an} (\mathbf{I} - \hat{\mathbf{q}}_i \hat{\mathbf{q}}_i^T) + C_{at} (\hat{\mathbf{q}}_i \hat{\mathbf{q}}_i^T) \right] \quad (2.20)$$

Now, the entire equation of motion per node may be written as

$$\underbrace{\mathbf{m}_i + \mathbf{a}_i}_{\text{mass and added mass}} \ddot{\mathbf{r}}_i = \underbrace{\mathbf{T}_{i+(1/2)} - \mathbf{T}_{i-(1/2)} + \mathbf{C}_{i+(1/2)} - \mathbf{C}_{i-(1/2)}}_{\text{internal stiffness and damping}} + \underbrace{\mathbf{W}_i + \mathbf{B}_i}_{\text{weight and contact}} + \underbrace{\mathbf{D}_{\mathbf{p}i} + \mathbf{D}_{\mathbf{q}i}}_{\text{drag}}, \quad (2.21)$$

which is a second-order ordinary differential equation (ODE). This equation can be reduced to a first-order ODE and solved using the Runge-Kutta (RK2) integration algorithm Hall and Goupee (2015).

2.5.4. Initial Cable Configuration

Before the mooring dynamics of the lines are solved, it is necessary to first determine the initial configuration of the line. This configuration is usually determined by equations that determine the position of all points (nodes) along the line. Figure 2.14 shows the mooring line in the local coordinate system. Here, the coordinate along the line length is designated s .

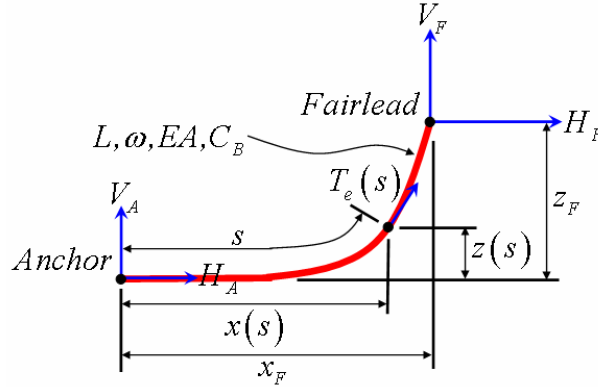


Figure 2.14: Mooring line in a local coordinate system (Jonkman, 2007).

Jonkman (2007) presented several equations to accomplish this. First, it is necessary to determine the horizontal and vertical components of the tension at the fairlead (H_F and V_F). The horizontal and vertical components of the tension with the mooring line having no seabed contact may be computed using the systems of equations presented in Equation 2.22 and Equation 2.23

$$x_F(H_F, V_F) = \frac{H_F}{\omega} \left\{ \ln \left[\frac{V_F}{H_F} + \sqrt{1 + \left(\frac{V_F}{H_F} \right)^2} \right] - \ln \left[\frac{V_F - \omega L}{H_F} + \sqrt{1 + \left(\frac{V_F - \omega L}{H_F} \right)^2} \right] \right\} + \frac{H_F L}{EA} \quad (2.22)$$

$$z_F(H_F, V_F) = \frac{H_F}{\omega} \left[\sqrt{1 + \left(\frac{V_F}{H_F}\right)^2} - \sqrt{1 + \left(\frac{V_F - \omega L}{H_F}\right)^2} \right] + \frac{1}{EA} \left(V_F L - \frac{\omega L^2}{2} \right), \quad (2.23)$$

where

x_F and z_F are the coordinates of the node at the fairlead,

ω is the mass per unit length of the line,

L is the length of the line,

EA is the axial stiffness of the line.

Equation 2.22 and Equation 2.23 needs to be solved iteratively (using Newton-Raphson solution scheme for example) to determine the values of V_F and H_F . Similarly, for lines with seabed contact, the vertical and horizontal components of the tension at the fairlead may be computed using the following systems to non-linear equations (Equation 2.24 and Equation 2.25)

$$\begin{aligned} x_F(H_F, V_F) = L - \frac{V_F}{\omega} + \frac{H_F}{\omega} \ln \left[\frac{V_F}{H_F} + \sqrt{1 + \left(\frac{V_F}{H_F}\right)^2} \right] + \frac{H_F L}{EA} \\ + \frac{C_B \omega}{2EA} \left[-\left(L - \frac{V_F}{\omega}\right)^2 + \left(L - \frac{V_F}{\omega} - \frac{H_F}{C_B \omega}\right) \max\left(L - \frac{V_F}{\omega} - \frac{H_F}{C_B \omega}, 0\right) \right] \end{aligned} \quad (2.24)$$

$$z_F(H_F, V_F) = \frac{H_F}{\omega} \left[\sqrt{1 + \left(\frac{V_F}{H_F}\right)^2} - \sqrt{1 + \left(\frac{V_F - \omega L}{H_F}\right)^2} \right] + \frac{1}{EA} \left(V_F L - \frac{\omega L^2}{2} \right), \quad (2.25)$$

where C_B is the seabed friction. As mentioned earlier, a non-linear solution scheme is needed to solve equations 2.22, 2.23, 2.24, and 2.25. To do this, a starting value (guess) is required; Peyrot and Goulois presented the starting values as shown in Equation 2.26 and Equation 2.27 (Jonkman, 2007)

$$H_F^0 = \left| \frac{\omega x_F}{2\lambda_0} \right| \quad (2.26)$$

$$V_F^0 = \frac{\omega}{2} \left[\frac{z_F}{\tanh(\lambda_0)} + L \right]. \quad (2.27)$$

λ_0 is a parameter which is determined according to the following rule:

$$\begin{cases} 1000000 & \text{for } x_F = 0 \\ 0.2 & \text{for } \sqrt{x_F^2 + z_F^2} \geq L \\ \sqrt{3 \left(\frac{L^2 - z_F^2}{x_F^2} - 1 \right)} & \text{otherwise} \end{cases} \quad (2.28)$$

Once H_F and V_F have been determined, then the horizontal and vertical tension of the line at the anchor may be determined by considering the equilibrium of the line. After the tension in the line at the anchor and fairlead are known for the particular time step under consideration has been determined, then the location of each node $(x(s), z(s))$ (after discretization) on the mooring line may now be computed using

$$x(s) = \frac{H_F}{\omega} \left\{ \ln \left[\frac{V_A + \omega s}{H_F} + \sqrt{1 + \left(\frac{V_A + \omega s}{H_F} \right)^2} \right] - \ln \left[\frac{V_A}{H_F} + \sqrt{1 + \left(\frac{V_A}{H_F} \right)^2} \right] \right\} + \frac{H_F s}{EA} \quad (2.29)$$

$$z(s) = \frac{H_F}{\omega} \left[\sqrt{1 + \left(\frac{V_A + \omega s}{H_F} \right)^2} - \sqrt{1 + \left(\frac{V_A}{H_F} \right)^2} \right] + \frac{1}{EA} \left(V_A s + \frac{\omega s^2}{2} \right) \quad (2.30)$$

The mooring system considered in this report is a taut system; therefore, there is no contact between the mooring lines and the sea floor. The equation to compute the position of the nodes along the lines for a cable making contact with the sea floor can be found in (Jonkman, 2007).

2.5.5. Modelling Fibre Ropes

The method described thus far is for a linear mooring line, such as steel chains and wires. Mooring lines made of materials such as polyester and nylon have nonlinear behaviour, and the method of calculating the tension is slightly different. Different classification societies and regulatory bodies propose different methods for considering the nonlinear tension strain relationship in a fibre rope. These methods were summarised in a table by West et al. (2020) and have been reproduced here in Table 2.5. As this work is still a preliminary design and not all the wind turbine data are currently available, the Upper-Lower bound model is used. At a later stage when more precise inputs such as the controller properties and the WTG tower are available, a non-linear analysis that takes into account the nonlinearity in the cable is included in the analysis. Further discussion on the Upper-Lower bound model and the determination of the numerical values are presented in subsubsection 4.7.3.

Table 2.5: Summary of recommended stiffness methods West et al. (2020).

Model name	Model Description	Code agency
Static dynamic model	The static stiffness is lower and used up to a mean loading. Then from the mean loading, a stiffer dynamic stiffness is utilised	ABS
Upper-Lower Bound Model	Here, two stiffness are chosen. The upper bound is the stiffer, and the lower bound is the expected soft stiffness. The analysis runs for both cases, and the maximum platform offset and cable tension are found. The actual system will lie somewhere between the lower and upper bound stiffness	ABS and API
Nonlinear Viscoelastic	The mooring lines are modelled as different viscoelastic setups such as the Generalised Maxwell Model and the Kelvin Model. Springs and dampers connected in series and parallel make up the model and give a realistic response.	DNV
Nonlinear load elongation model	A lookup table containing the Load-Elongation relationship or analytical relationship is used to model the load-elongation relationship	API
Separate decoupled frequency responses	Responses due to high-frequency wind loads, current and wind loads, low-frequency wave, and mean environmental loading are evaluated, and the responses are added together.	API

3. METHODOLOGY

3.1. Software Selection

The software applications used for this analysis are open-source due to the limitations of student licenses of commercially available software applications. The good thing about open source is that it has more capabilities and draws the user closer to the underlying theories. Open-source's strength is that it requires a more in-depth understanding and a sound user to run it. Commercial software is a black box that can be used to generate results by any random user. The major stages in the analysis are geometry creation, mesh generation, frequency domain analysis, and time domain analysis with the mooring lines attached to the platform. The major open-sourced software applications used for this thesis are capytaine, WEC-Sim, NEMOH, BEMRosetta, and OpenFAST. Capytaine is used for the frequency domain analysis of the floater without the mooring lines as a first step in gaining some insight into the problem, while WEC-Sim is used for the time series analysis to compute the response of the platform with different mooring configurations (only surge, heave and pitch responses are possible). After fully understanding the problem, OpenFAST, NEMOH and BEMRosetta are used to compute the system response in yaw.

3.1.1. AutoCAD and Rhinoceros

AutoCAD is a computer-aided design (CAD) and drafting software created by Autodesk to produce 2D and 3D drawings. Due to the relative ease of using this drafting software, it is used to reproduce the 2D geometry of the spar. The 2D geometry is then exported to Rhinoceros to create a 3D step file and meshed parts.

3.1.2. GMSH

GMSH is an open-source meshing generator developed by Christophe Geuzaine and Jean-François Remacle (Geuzaine and Remacle, 2009). The program contains four modules: the geometry module, meshing module, solving module, and post-processing module. The 3D step file created in Rhino is merged with a new .geo file in GMSH. This geometry file is then meshed and saved as a .stl format for use in Capytaine.

3.1.3. Capytaine

Capytaine software, a Python-based potential flow solver, simulates the interaction between wind, waves and a floating body in the frequency domain. Capytaine is a Python version of NEMOH (which was written in FORTRAN), and the output generated by this program can also be generated using AQWA and WAMIT. However, due to the license requirements of AQWA and WAMIT, they are not considered for this analysis.

Figure 3.1 shows the method followed in Capytaine to compute the hydrodynamic forces. In orange are the required inputs. In blue are the processes required to produce the result in yellow. The v 2.0 of the program was used for this study, and the major Python compilers used are ipython, qtconsole, and jupyter notebook. Capytaine is first used to understand the problem better and to provide the necessary input files for WEC-Sim. While NEMOH and BEMRosetta are used to prepare the hydrodynamic input file for OpenFAST.

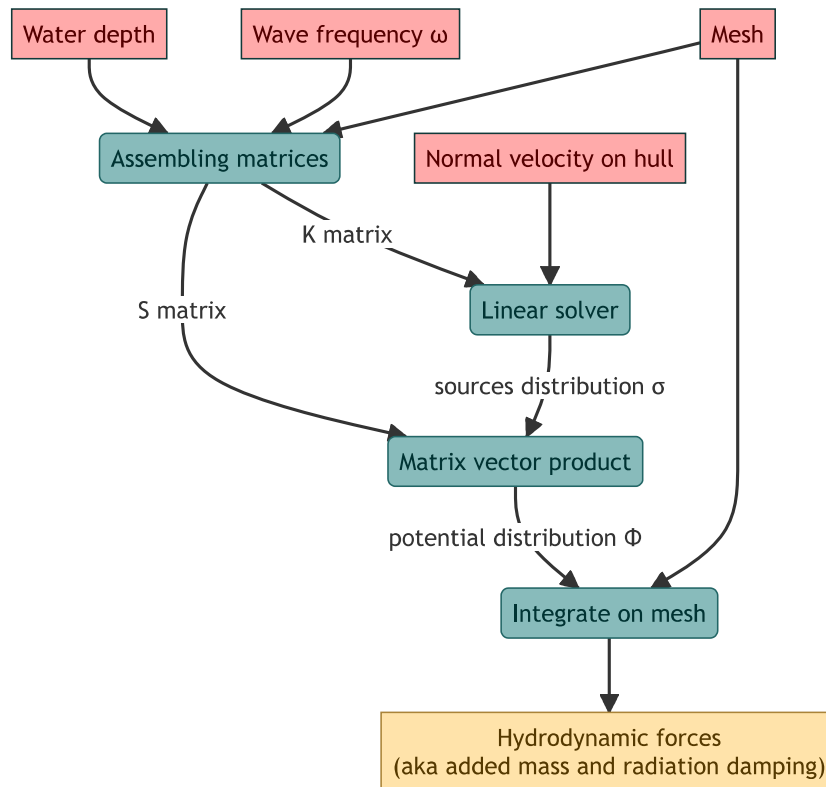


Figure 3.1: Simplified flowchart of the internals of Capytaine solver (Ancellin, 2023).

The time it takes Capytaine to run depends on the input size given. For example, a finer mesh or a higher frequency range with many data points will require more computational power. The finest mesh possible is used in this work since only one run of the complete solution in Capytaine is required.

3.1.4. NEMOH

NEMMOH is a BEM code developed by a group of researchers in Ecole Central de Nantes over 30 years ago and was first released in 2014. This program is used to compute wave loads on offshore structures, such as added mass, radiation damping and diffraction forces (Kurnia and Ducrozet, 2022). The current release, v3, has two modules, NEMOH1 for first-order computation and NEMOH2 for computing the quadratic transfer function (QTF). The flowchart of the software is shown in Figure 3.2.

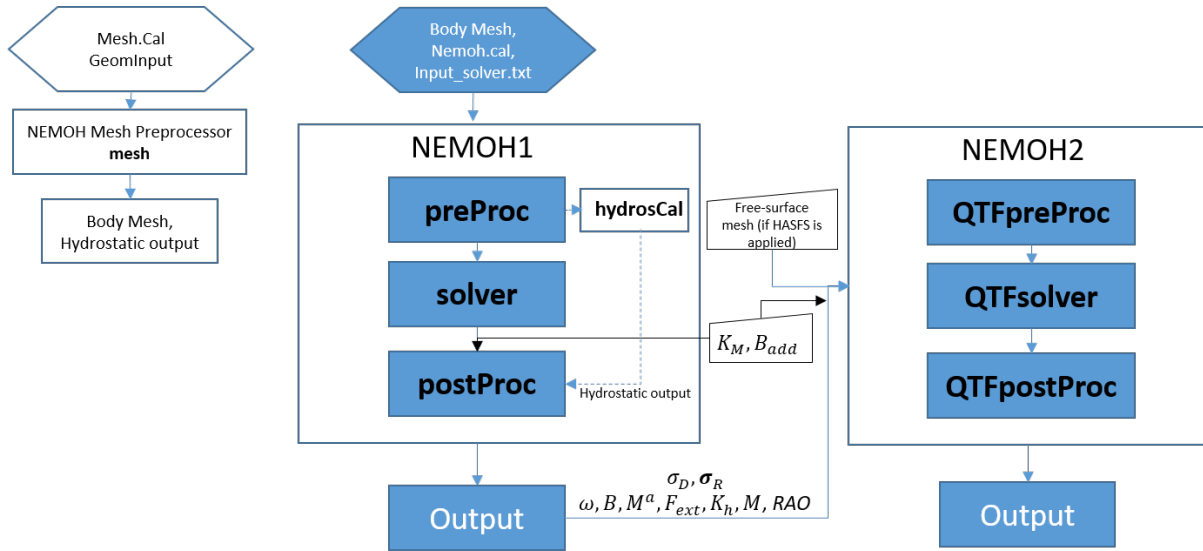


Figure 3.2: Global flowchart of NEMOH software (Kurnia and Ducrozet, 2022).

The output from NEMOH can not be read directly by OpenFAST, so the software BEMRosetta was used to convert the output to a WAMIT-style output.

3.1.5. BEMRosetta

BEMRosetta, a software developed by (Zabala et al., 2021), is used to convert the BEM output from one program to the format of another program. For example, in this work, the out of the NEHMOH is in *.tec* format is converted to WAMIT format (*.1*, *.3*, and *.hst*) which is the only output OpenFAST can read. Viewing the BEM using BEMRosetta is also possible.

3.1.6. MoorDyn

MoorDyn is an open-source lumped mass mooring model used for predicting the dynamics of a mooring line without considering bending and torsional stiffness (Hall, 2015). This definition only applies to version 1 of the program as it is now possible to consider bending stiffness on v2. The v1 is used with WEC-Sim since this is the only version that works with it, while the version 2 is used with OpenFAST. Even though the v2 is used with OpenFAST, as already mentioned in subsection 2.5.3, the bending stiffness is not considered for the lines and is neglected for this preliminary stage of the design process. The program's primary purpose is coupling with other solvers such as WEC-Sim, OpenFAST, DualSPysics, OPENFoam, and STARCCM+. It is also possible to use the program as a standalone, whereby the fairlead motion is supplied as input based on some mathematical functions. A sinusoidal movement, for example, can be represented by a sine or cosine function. In order to couple MoorDyn and WEC-Sim with a Windows operating system, the source code of MoorDyn needs to be compiled into a dynamically

linked library (dll). This dll and MoorDyn header file are the two files required for coupling MoorDyn with WEC-Sim. For the mooring design, the MoorDyn was selected since it is possible to couple it with the WEC-Sim application.

3.1.7. OpenFAST

OpenFAST is a program that couples the aerodynamic-, hydrodynamic-, and structural response of a floating platform with the Coriolis effect of the generators and the mooring dynamics of the station-keeping systems. More details about this program is provided in subsection 3.3.

3.1.8. WEC-Sim

The wave energy converter simulator is an open-source software developed in MATLAB/Simulink using the multi-body dynamics solver Simscape Multi-body. Although WEC-Sim is primary for designing a wave energy converter, it is also suitable for designing the mooring system of any floating body if the correct inputs are provided. WEC-Sim only simulates the interaction between the floating body and waves the addition of wind load or WTG forcing function is not possible. In this work, WEC-Sim is used as a starting point in understanding a wind turbine's time series coupled simulation. Though the superstructure is not present, it serves as an academic exercise. It gives an insight into how MoorDyn coupling works since MoorDyn is the mooring dynamics code used with OpenFAST in this work.

A geometry in *.stl* meshed format is required for the simulation. When a linear analysis is performed, this geometry is used just for animation, so the meshing does not matter. However, if the analysis is a non-linear one, then the size of the mesh of the geometry will play a significant role (Ogden et al., 2022). In this study, only a linear analysis is done, so a coarse mesh saves computational time. Figure 3.3 shows input parameters of WEC-Sim and the BEMIO. The PTO is not taken into consideration for this work; therefore, the PTO-Sim module is not added in the Simulink model and the WEC-Sim input file. In the pre-analysis, the BEM code used is Capytaine, a linear analysis for the hydrodynamics. A user-defined wave time series obtained from Parkwind nv is used (the FLS 351, 365, and 390). Each time series represents a one-hour elevation record with a time step of 0.025 s. More details about the elevation record in subsubsection 4.9.1. The mooring code used is MoorDyn, and the visualization software is Paraview. The various modules in the Simulink library are shown in subsection 4.6. These are needed to build the model required for analysis as seen in subsection 4.6.

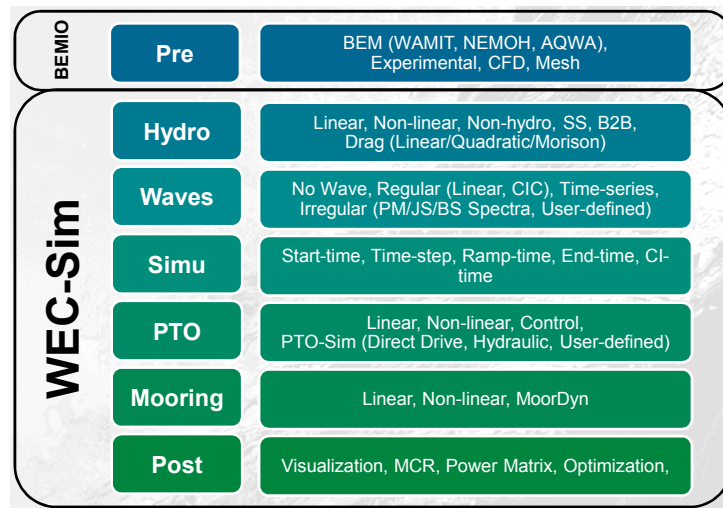


Figure 3.3: WEC-Sim input parameters (Ruehl, 2017).

The model is built by dragging the sub-module from each module. For example, the spar floater *.stl* geometry file is assigned to the body element, and DOFs are assigned to the constraints. The frame is used to assign the seabed while the MoorDyn is assigned to the Mooring module. In this work, only four modules are used: the body elements, constraints, frames, and moorings. The eventual model created must be saved in the same directory as the WEC-Sim input file or in any other location provided the WEC-Sim input file is modified to point to the directory where it is saved.

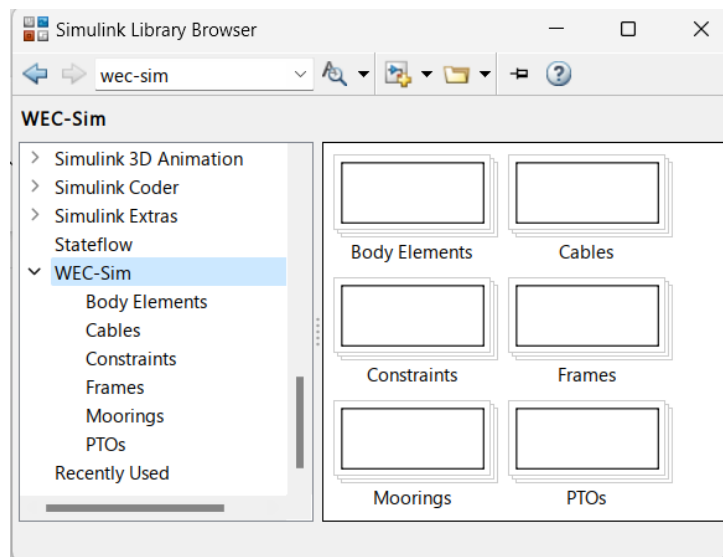


Figure 3.4: Simulink library.

3.2. WEC-Sim Solution Strategy

This section describes the method WEC-Sim uses to carry out the mooring design. Figure 3.5 presents the program flow, which shows the input files needed, the required stage, and the processes needed to give the desired output at the extreme right of the

flowchart. One of the input files is the geometry file, which must be provided in a *.stl* file format with the global frame of reference positioned at the cog. This geometry differs from the one Capytaine uses for the potential flow solution. For the geometry used in Capytaine, the global reference plane is positioned at the mean sea level (MSL) along the axis of the vertical cog. The BEM code used is Capytaine, a Python-based application described in subsection 3.1.3. The output of Capytaine is parsed to WEC-Sim as a NetCDF. The boundary element input/output (BEMIO) receives this input from Capytaine and converts it to a hierarchical data format (*.h5*), which is then parsed to the next stage of the program analysis run.

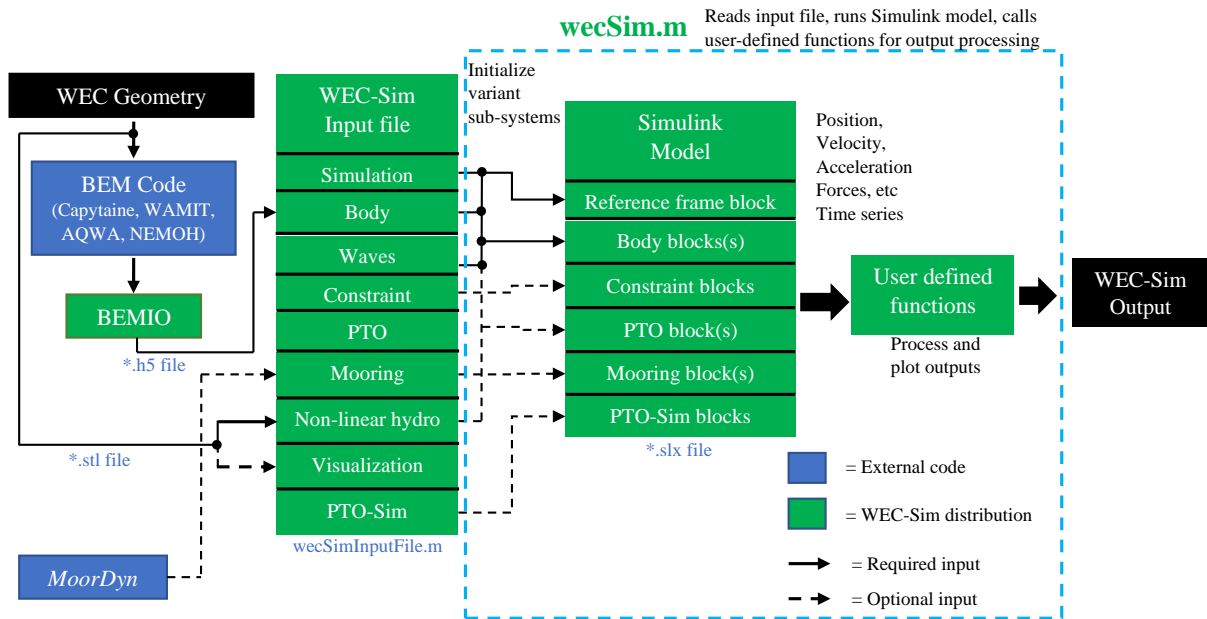


Figure 3.5: Flow chart of WEC-Sim (Ruehl et al., 2022).

The MoorDyn input file is a text file containing the properties of the mooring lines. This text file is in a sub-folder named *Mooring* in the WEC-Sim directory. A brief description of the BEM solution, MoorDyn coupling, and the equation of motion solved by WEC-Sim is presented next.

3.2.1. Boundary Element Method Solution

The method adopted by the capytaine program for solving the radiation and diffraction problem is the Boundary Element Method. In this method, the following assumptions are made:

- Sea bottom is flat.
- The wave amplitude is small compared to the wavelength, which implies a small slope.
- The fluid is inviscid.

- The flow is irrotational and incompressible.

The irrotational and inviscid flow means Airy's wave theory is applicable. The Le Méhauté's diagram discussed in subsection 2.3.2 justifies using Airy's wave theory. The water depth of the wind farm location is 250 m. The flow can be considered inviscid since flow separation is less dominant, hence negligible drag.

3.2.2. Time Series Solution Methodology with WEC-Sim

The WEC-Sim software outputs the platform's response, displacement, velocity, and acceleration by solving the Cummins equation. This equation is represented as:

$$m\ddot{X} = F_{exc}(t) + F_{md}(t) + F_{rad}(t) + F_{pto}(t) + F_v(t) + F_{me}(t) + F_B(t) + F_m(t) \quad (3.1)$$

Where:

- \ddot{X} is the translation and rotation acceleration vector of the platform
- $F_{exc}(t)$ wave excitation force and torque vector
- $F_{md}(t)$ mean drift force and torque vector
- $F_{rad}(t)$ Force and torque vector resulting from wave radiation
- $F_{pto}(t)$ Power take-off force and torque vector
- $F_v(t)$ Damping force and torque vector
- $F_{me}(t)$ Morison element force and torque vector
- $F_B(t)$ Net buoyancy restoring force and torque vector
- $F_m(t)$ Force and torque vector resulting from mooring connection

For the current platform under consideration, the mean drift and power take-off force and torque will not be taken into account so that the equation of motion reduces to

$$m\ddot{X} = F_{exc}(t) + F_{rad}(t) + F_v(t) + F_{me}(t) + F_B(t) + F_m(t). \quad (3.2)$$

Where each term maintains the same meaning as those in Equation 3.1. The $F_{exc}(t)$ and $F_v(t)$ terms of Equation 3.1 are inputs to WEC-Sim which are generated by the BEM software such as Capytaine as in the case of this thesis.

3.2.3. Coupling with MoorDyn

In MoorDyn, there is a possibility of using different types of mooring materials, such as polyester and chains or the same materials with different properties. The point where two different materials meet is a special node called *connect*. The *connect* nodes are not fixed

in space but move according to the force acting on them. There are two other types of special nodes, namely: *vessel*, which moves under the control of an outside program. This node is mainly used to specify a point on the fairlead. The second one is the *fixed* node; this node does not move and is usually used to specify the anchor point (Hall, 2015). The *.txt* file input format of MoorDyn is shown in Figure 3.6.

```

Mooring line data file for MoorDyn in Lines.dll
----- LINE DICTIONARY -----
LineType Diam MassDenInAir EA BA/-zeta Can Cat Cdn Cdt
(-) (m) (kg/m) (N) (Pa-s/-) (-) (-) (-) (-)
----- NODE PROPERTIES -----
Node Type X Y Z M V FX FY FZ CdA CA
(-) (-) (m) (m) (m) (kg) (m^3) (kN) (kN) (kN) (m^2) (-)
----- LINE PROPERTIES -----
Line LineType UnstrLen NumSegs NodeAnch NodeFair Flags/Outputs
(-) (-) (m) (-) (-) (-) (-)
----- SOLVER OPTIONS -----
x1 dtM - time step to use in mooring integration
x2 WaveKin - wave kinematics flag (0=neglect the only option currently supported)
x3 kBot - bottom stiffness
x4 cBot - bottom damping
x5 WtrDpth - water depth
x6 CdScaleIC - factor by which to scale drag coefficients during dynamic relaxation IC gen
x7 threshIC - threshold for IC con
x8 WriteUnits - option to skip units line in output files if zero
----- OUTPUTS -----
----- need this line -----

```

Figure 3.6: MoorDyn Input file.

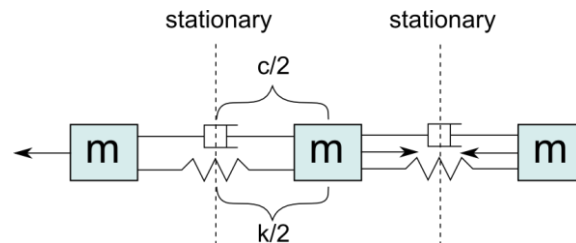
The input file is divided into different sections. The sections are *LINE DICTIONARY*, *NODE PROPERTIES*, *SOLVER OPTIONS*, and *OUTPUTS*. In the *LINE DICTIONARY*, the properties of the lines are specified. At the same time, the properties of the connected nodes are described in the *NODE PROPERTIES* section. In the *OUTPUT* section, the user specifies the desired output of the MoorDyn program. The list of possible outputs is presented in Hall (2015). The meaning of each parameter is already described in the figure for the *SOLVER* option. The *x1*, *x2*, ..., and *x8* under the *SOLVER OPTIONS* are placeholders for numbers. The meaning of the rest of the terminologies is shown in Table 3.1, and the procedure for determining their numerical values is done in subsection 4.7.

In Table 4.3, the unit of the line internal damping is [Pa s] or [-], because in MoorDyn it is possible to enter the absolute value of the internal damping stiffness, in which case the unit is [Pa s], or a negative decimal number (which represents a fraction of the critical damping) can be entered in which case, the internal damping will have no unit. This internal damping parameter damps out the *artificial* resonance created by the line discretisation.

Table 3.1: MoorDyn parameter description.

Parameter	Description [units]
LineType	Word for line type ID, eg chain, polyester [-]
Diam	volume equivalent diameter of the line [m]
MassDenInAir	Dry mass per unit length of the line [kg m^{-1}]
EA	Axial stiffness of the line [N]
$BA/ - zeta$	Line internal damping [Pa-s] or [-]
C_{an}	Transverse added mass coefficient [-]
C_{at}	Tangential added mass coefficient [-]
C_{dn}	Transverse drag coefficient [-]
C_{dt}	Tangential drag coefficient [-]
Node	ID of the nodal connection [-]
Type	connect, fix or vessel [-]
X, Y, Z	Coordinates of the nodes [m]
M	Node mass of clump weight at the node [kg]
V	Node displacement at the node for floats [m^3]
FX, FY, FZ	Steady external force applied at the node [N]
C_{dA}	Product of projected area by drag coefficient [m^2]
C_a	Added mass coefficient used along with V [-]
UnstrLen	Unstretched length of the line [m]
NumSegs	Number of segments of the line [-]
NodeAnch	ID of the node of a line segment close to anchor [-]

Most of the input files of MoorDyn are straightforward, but BA and dtM , which are related to the line discretisation, are tricky parameters (Hall, 2015). To consider BA , Hall (2015) presented a simple approach by considering the line as a spring-damper system. Figure 3.7 shows the discretised line as a simple mass spring damper. The maximum axial vibration mode will occur when two adjacent masses vibrate out of phase, making the line's midpoint remain stationary (Hall, 2015).

**Figure 3.7:** Mass spring damper idealisation of the mooring line (Hall, 2015).

With the system presented in Figure 3.7, the mass of each node (m) may be presented as a fraction of the total mass of the line (wL), where L is the total length of the line and w

is the distributed weight of the line. According to Hall (2015), the natural frequency and damping of the line may be represented respectively as

$$\omega_n = \frac{2N}{L} \sqrt{\frac{EA}{w}} \quad (3.3)$$

$$BA = \zeta \frac{L}{N} \sqrt{EAw}, \quad (3.4)$$

where ζ is the damping ratio of the line and EA is the axial stiffness. It is recommended that the damping ratio be close to 1 as much as possible to damp out the resonance frequency of the line segment to ensure that the model is resolved properly. For simplicity, Hall (2015) recommended that the negative value be entered in this section of the input file ($BA/ -zeta$) to give the damping ratio of each line segment. This approach is adopted here; only the global behaviour of the line is sorted.

3.3. OpenFAST Solution Strategy

To analyse the mooring configuration in the yaw DOF, it is necessary to analyze with a code capable of perturbing the wind turbine in the yaw. Since WEC-Sim does not provide this possibility, OpenFAST is used. OpenFAST is an aero-servo-hydro-elastic solver used for computing the response of floating platforms. The IEA 15 MW offshore reference model on UMaine VoltturnUS-S semi-submersible floating platform is adapted in this work. The various modules used in OpenFAST are shown in Figure 3.8.

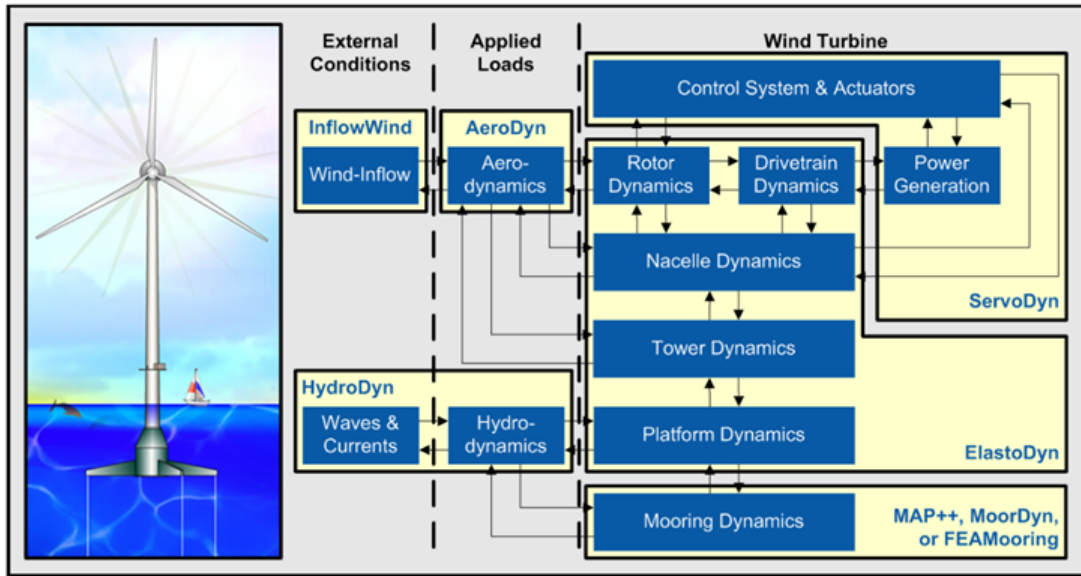


Figure 3.8: FAST control volumes for floating systems (Jonkman and Jonkman, 2016).

The OpenFAST.exe is a glue code that binds all the modules shown in Figure 3.8. The external conditions are defined in InflowWind (wind) and HydroDyn (waves and current). Then, AeroDyn interacts with the outputs generated from the Inflow wind to compute the applied loads on the wind turbine's blades. In the HydroDyn, the hydrodynamic loads are also computed for each time step. There is the possibility of computing the hydrodynamic coefficients using a BEM code such as NEMOH and WAMIT. This work uses NEMOH to carry out the BEM analysis. The control system of the generator and actuator systems are defined in ServoDyn. Then, the tower, platform, and nacelle dynamics are defined in the ElastoDyn input file. Moreover, finally, the mooring dynamics are described in MAP++, MoorDyn, or FEMooring. In this work, MoorDyn is used. Other modules, such as IceDyn and SubDyn are also available in OpenFAST. SubDyn is used for a fixed platform, while IceDyn considers surface ice on the wind turbine (not considered here to simplify the analysis).

In this work, the OpenFAST v3.5.0 is used, and the MoorDyn version coupled with it is v2. The input file of v2 MoorDyn is significantly different from the ones described in subsection 3.2.3 due to the added functionality. However, considering the scope of

this work, the inputs for both v_1 and v_2 are identical since non-linearity in the line is not considered.

3.3.1. HydroDyn Calculation Procedure

The HydroDyn calculation procedure is presented in Figure 3.9.

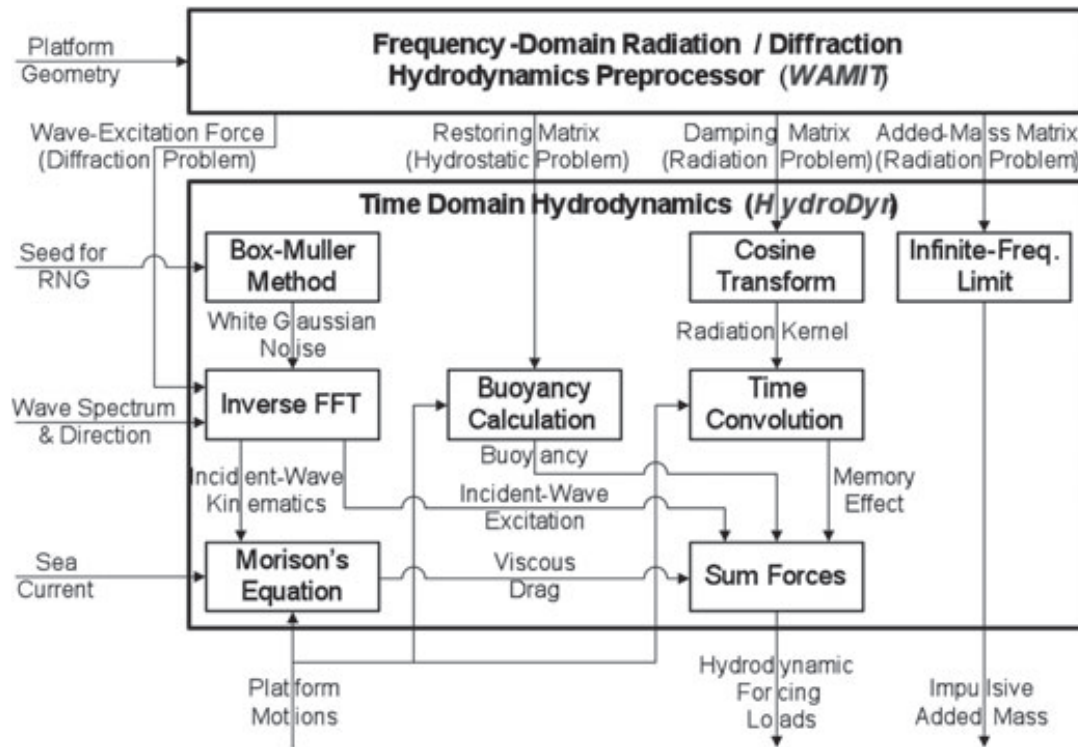


Figure 3.9: HydroDyn Calculation Procedure (Jonkman, 2009).

6. CONCLUSION AND RECOMMENDATIONS

6.1. Conclusion

The results of the hydrostatics obtained for the spar geometry align with what was expected. However, a disparity in the wind turbine structure's total mass was observed after adding the individual masses of the wind turbine, which did not match the displaced mass. This difference in weight was accounted for by adding weight to the solid ballast, and the cog adjusted accordingly. The results obtained for the BEM analysis for the radiation damping and added mass align with what was expected. The radiation damping and added mass for each of the DOF approached zero and a fixed value, respectively, at infinite frequency. The mooring configuration was designed by adapting the IEA 15 MW semi-submersible wind turbine data to the spar. A fully coupled analysis was done in the time domain using wave elevation records from Utsira Nord. The chosen configuration is a three-line semi-taut configuration with better yaw stiffness than the proposed configuration of Olsen (2022). Also, the new configuration makes efficient use of materials by using 30% and 50% less polyester and chain lines, respectively.

6.2. Recommendations

It would be interesting to verify and validate some of the results obtained in this work. Also, given more time, a different analysis approach can be followed. The following recommendations are suggested

- The through non-linear viscoelastic behaviour of the polyester mooring line should be modelled for calculating the mooring line tension.
 - Shared mooring design should be assessed using fast farm.
 - The coupled analysis should be done with the accurate data of the controller, site-specific wind data should be used, and the correct tower bending modes and inertia should be used for the analysis after all the data are made available.
 - If possible, results obtained should be validated by tank testing.
 - A coupled computational fluid dynamics (CFD) analysis should be done to verify the results obtained.
-

ACKNOWLEDGEMENTS

My heartfelt appreciation goes to God Almighty for making this thesis a success. I am grateful to my supervisors, Griet Decorte and Tomas Lopez, for their immense help throughout the thesis period. They both provided the needed support and encouragement all through. Special thanks to my lovely wife, Dorcas Olaiya, for continuously checking up on me and for her moral support. I will not fail to appreciate my family and friends for their show of love during this period. In no particular order, I say a special thanks to David Ajiboye, Stella Ajiboye, Florence Eseyin, Tope Ajiboye, and Segun Ajiboye, who are an essential part of my family, for the love they showed me and the belief they have in me. Posterity will fail me without appreciating my EMShip friends: De Oliveira Vieira Marcos Vinicius, Al-Ghuwaidi Abdulelah, Mertens Neil, Pangpun Papatsornpun, Jorge Alcantara Felipe, Oconnor Declan, Mosciatti Urzua Ezio Antonio. My association with them made the EMShip journey an enjoyable one. Finally, a special thanks goes to the EMShip coordinator, Prof. Rigo and the EMShip coordinator at UPM, Asst. Prof. Simone Saettone for making this programme possible. Also, I am thankful to the European Union for sponsoring my studies throughout the two years.

References

- Abbasi, K. R. and Adedoyin, F. F. (2021). Do energy use and economic policy uncertainty affect co 2 emissions in china? empirical evidence from the dynamic ardl simulation approach. *Environmental Science and Pollution Research*, 28:23323–23335.
- Abbasi, K. R., Adedoyin, F. F., Abbas, J., and Hussain, K. (2021). The impact of energy depletion and renewable energy on co2 emissions in thailand: fresh evidence from the novel dynamic ardl simulation. *Renewable Energy*, 180:1439–1450.
- ABS (2021). Guidance notes on the application of fiber rope for offshore mooring.
- Acteon (2015). *InterMoor Product Manual*. Acteon. Accessed on July 10, 2023.
- Ali, M. O. A., Ja’e, I. A., and Hwa, M. G. Z. (2020). Effects of water depth, mooring line diameter and hydrodynamic coefficients on the behaviour of deepwater fpsos. *Ain Shams Engineering Journal*, 11(3):727–739.
- Ancellin, M. (2023). Capytaine - theory manual. https://ancell.in/capytaine/latest/theory_manual/theory.html. Accessed: July 1, 2023.
- Ancellin, M. and Dias, F. (2019). Capytaine: a python-based linear potential flow solver. *Journal of Open Source Software*, 4(36):1341.
- API (2001). API Recommended Practice 2SM Design, Manufacture, Installation, and Maintenance of Synthetic Fiber Ropes for Offshore Mooring.
- API (2014). Api recommended practice 2sm design, manufacture, installation, and maintenance of synthetic fiber ropes for offshore mooring.
- Azcona Armendáriz, J. (2015). *Computational and Experimental Modelling of Mooring Lines Dynamics for Offshore Floating Wind Turbines*. PhD thesis, Navales.
- Benitz, M. A., Lackner, M., and Schmidt, D. (2015). Hydrodynamics of offshore structures with specific focus on wind energy applications. *Renewable and Sustainable Energy Reviews*, 44:692–716.
- Bergdahl, L. (2017). Mooring design for wecs. *Handbook of Ocean Wave Energy*, page 159.
- Bhinder, M. A., Karimirad, M., Weller, S., Debruyne, Y., Guérinel, M., and Sheng, W. (2015). Modelling mooring line non-linearities (material and geometric effects) for a wave energy converter using aqwa, sima and orcaflex. In *Proceedings of the 11th European wave and tidal energy conference, Nantes, France*, pages 6–11.
-

- Calderon-Sanchez, J. (2023). Hydrodynamic forces and motions in floating and fixed structures subjected to wave loads. Lecture Slides. Lecture presented at universidad politecnica de madrid, Spain.
- Castello, X. (2021). Floating offshore spar wind turbine in ansys aqwa - from a sketch to numerical model. Video file. Retrieved from <https://youtu.be/XthkX7pqfew>.
- Ćatipović, I., Čorić, V., and Radanović, J. (2011). An improved stiffness model for polyester mooring lines. *Brodogradnja: Teorija i praksa brodogradnje i pomorske tehnike*, 62(3):235–248.
- Chakrabarti, S. K. (1987). *Hydrodynamics of offshore structures*. WIT press.
- DNV (2010a). Environmental conditions and environmental loads. Technical report, DNV-RP-C205, DNV.
- DNV (2010b). Global performance analysis of deepwater floating structures. Technical report, DNV-RP-F205, DNV.
- DNV (2011). Modelling and analysis of marine operations, recommended practice: Dnv-rp-h103.
- DNV, G. (2018a). Floating wind turbine structures: Dnvgl-st-0119.
- DNV, G. (2018b). Offshore standard-position mooring (dnvgl-os-e301). *Edition July*.
- El Beshbichi, O., Xing, Y., and Ong, M. C. (2022). Comparative dynamic analysis of two-rotor wind turbine on spar-type, semi-submersible, and tension-leg floating platforms. *Ocean Engineering*, 266:112926.
- Equinor (2021). Vårgrønn to deliver technology for floating wind project on Utsira Nord. <https://www.equinor.com/news/archive/20210506-vaargroenn-floating-wind-utsira-nord>. Accessed on June 25, 2023.
- Faltinsen, O. (1993). *Sea loads on ships and offshore structures*, volume 1. Cambridge university press.
- Geuzaine, C. and Remacle, J.-F. (2009). Gmsh: a three-dimensional finite element mesh generator with built-in pre- and post-processing facilities. *International Journal for Numerical Methods in Engineering*, 79(11).
- Hall, M. (2015). Moordyn user’s guide. *Department of Mechanical Engineering, University of Maine: Orono, ME, USA*, 15.
- Hall, M. and Goupee, A. (2015). Validation of a lumped-mass mooring line model with deepcwind semisubmersible model test data. *Ocean Engineering*, 104:590–603.
-

- Holthuijsen, L. H. (2010). *Waves in oceanic and coastal waters*. Cambridge university press.
- IRENA (2021). Renewable power generation costs in 2021 [online]. Retrieved from https://www.irena.org/-/media/Files/IRENA/Agency/Publication/2022/Jul/IRENA_Power_Generation_Costs_2021.pdf?rev=34c22a4b244d434da0accde7de7c73d8. [Accessed: 28 May 2023].
- Jonkman, B. and Jonkman, J. (2016). Fast v8. 16.00 a-bjj. *National Renewable Energy Laboratory*, 1355.
- Jonkman, J. (2010). Definition of the floating system for phase iv of oc3. Technical report, National Renewable Energy Lab.(NREL), Golden, CO (United States).
- Jonkman, J. M. (2007). *Dynamics modeling and loads analysis of an offshore floating wind turbine*. University of Colorado at Boulder.
- Jonkman, J. M. (2009). Dynamics of offshore floating wind turbines—model development and verification. *Wind Energy: An International Journal for Progress and Applications in Wind Power Conversion Technology*, 12(5):459–492.
- Jonkman, J. M. and Matha, D. (2011). Dynamics of offshore floating wind turbines—analysis of three concepts. *Wind Energy*, 14(4):557–569.
- Journée, J. and Massie, W. (2001). Offshore hydromechanics. *Delft University of Technology*.
- Kausche, M., Adam, F., Dahlhaus, F., and Großmann, J. (2018). Floating offshore wind-economic and ecological challenges of a tlp solution. *Renewable Energy*, 126:270–280.
- Kurnia, R. and Ducrozet, G. (2022). Nemoh v3. 0 user manual. *Ecole Centrale de Nantes*.
- Lloyd, A. (1998). Seakeeping: Ship behaviour in rough weather. *ARJM Lloyd*.
- Martinez, A. and Iglesias, G. (2022). Mapping of the levelised cost of energy for floating offshore wind in the european atlantic. *Renewable and Sustainable Energy Reviews*, 154:111889.
- Musial, W., Duffy, P., Heimiller, D., and Beiter, P. (2021). Updated oregon floating offshore wind cost modeling [slides]. Technical report, National Renewable Energy Lab.(NREL), Golden, CO (United States).
- Ogden, D., Ruehl, K., Yu, Y.-H., Keester, A., Forbush, D., Leon, J., and Tom, N. (2022). Review of wec-sim development and applications. *International Marine Energy Journal*, 5(NREL/JA-5700-83366).
-

- Olsen, D. O. (2022). Concrete spar design for floating wind - utsira nord. Study Report 13586-OO-RIX-R-002, DR. TECHN OLAV OLSEN ARTELIA GROUP, Postboks 139, 1325 Lysaker, Norway. rev. 02.
- Orcina (nda). Chain: Added mass. Available online. Accessed: 2023-07-31.
- Orcina (ndb). Rope/wire: Axial and bending stiffness. Available online. Accessed: 2023-08-23.
- Paladhi, A. G., Vallinayagam, S., Rajendran, S., Rathinam, V., and Sharma, V. K. (2022). Microalgae: a promising tool for plastic degradation. In *Microbes and Microbial Biotechnology for Green Remediation*, pages 575–587. Elsevier.
- ProteusDS (2018). *ProteusDS Manual*. Dynamic Systems Analysis Ltd., Victoria, BC, Canada, v2.45 edition.
- Quallen, S., Xing, T., Carrica, P., Li, Y., and Xu, J. (2013). Cfd simulation of a floating offshore wind turbine system using a quasi-static crowfoot mooring-line model. In *ISOPE International Ocean and Polar Engineering Conference*, pages ISOPE–I. ISOPE.
- Rani, M., Shanker, U., et al. (2023). The role of nanomaterials in plastics biodegradability. In *Biodegradability of Conventional Plastics*, pages 283–308. Elsevier.
- Ridge, I., Banfield, S., and Mackay, J. (2010). Nylon fibre rope moorings for wave energy converters. In *OCEANS 2010 MTS/IEEE SEATTLE*, pages 1–10. IEEE.
- Ruehl, K., Ogden, D., Yu, Y.-H., Keester, A., Tom, N., Forbush, D., Leon, J., Grasberger, J., and Husain, S. (2022). Wec-sim v5.0.1.
- Ruehl, K. M. (2017). Wec-sim worksop. Technical report, Sandia National Lab.(SNL-NM), Albuquerque, NM (United States).
- Shittu, A. A., Mehmanparast, A., Hart, P., and Kolios, A. (2021). Comparative study between sn and fracture mechanics approach on reliability assessment of offshore wind turbine jacket foundations. *Reliability Engineering & System Safety*, 215:107838.
- Team, C. R. (2023). Everything about polyamide 6 you should to know (pa6 / nylon 6). Accessed on: [2023-08-16].
- Tran, T.-T. and Kim, D.-H. (2015). The platform pitching motion of floating offshore wind turbine: A preliminary unsteady aerodynamic analysis. *Journal of Wind Engineering and Industrial Aerodynamics*, 142:65–81.
- Vazquez, A. and Iglesias, G. (2016). Grid parity in tidal stream energy projects: An assessment of financial, technological and economic lcoe input parameters. *Technological forecasting and social change*, 104:89–101.
-

- Veritas, B. (2021). *NR493 - Classification of Mooring Systems for Permanent and Mobile Offshore Units*. Online.
- Vlasblom, M. (2018). The manufacture, properties, and applications of high-strength, high-modulus polyethylene fibers. In *Handbook of Properties of Textile and Technical Fibres*, pages 699–755. Elsevier.
- Wang, J.-h., Mamkhezri, J., Khezri, M., Karimi, M. S., and Khan, Y. A. (2022). Insights from european nations on the spatial impacts of renewable energy sources on co2 emissions. *Energy Reports*, 8:5620–5630.
- Weller, S., Davies, P., Johanning, L., and Banfield, S. (2013). Guidance on the use of synthetic fibre ropes for marine energy devices. *Marine Energy in Far Peripheral and Island Communities*.
- West, W., Goupee, A., Viselli, A., and Dagher, H. (2020). The influence of synthetic mooring line stiffness model type on global floating offshore wind turbine performance. In *Journal of physics: conference series*, volume 1452, page 012044. IOP Publishing.
- WindEurope (2017). Floating offshore wind vision statement [online]. Retrieved from <https://windeurope.org/wp-content/uploads/files/about-wind/reports/Floating-offshore-statement.pdf>. [Accessed: 28 May 2023].
- Zabala, I., Pena-Sanchez, Y., Kelly, T., Henriques, J., Penalba, M., Faedo, N., Ringwood, J., and Blanco, J. M. (2021). Bemrosetta: An open-source hydrodynamic coefficients converter and viewer integrated with nemoh and foamm. In *Proceedings of the 14th European Wave and Tidal Energy Conference 5-9th Sept 2021, Plymouth, UK*.
- Ørsted (n.d.). Floating offshore wind energy. Accessed: July 3, 2023.
-